The role of blocking circulation and emerging open water feedbacks on Greenland cold-season air temperature variability over the last century

Thomas J. Ballinger[1], Edward Hanna[2], Richard J. Hall[3], J. Rachel Carr[4], Saber Brasher[5], Erich C. Osterberg[6], John Cappelen[7], Marco Tedesco[8,9], Qinghua Ding[10], and Sebastian H. Mernild[11,12,13,14]

[1]International Arctic Research Center, University of Alaska Fairbanks, Fairbanks, AK, USA, tjballinger@alaska.edu
[2]School of Geography and Lincoln Centre for Water and Planetary Health, University of Lincoln, Lincoln, UK
[3]School of Geographical Sciences, University of Bristol, Bristol, UK
[4]School of Geography, Politics and Sociology, Newcastle University, Newcastle upon Tyne, UK
[5]Department of Geography and Spatial Sciences, University of Delaware, Newark, DE, USA
[6]Department of Earth Sciences, Dartmouth College, Hanover, NH, USA
[7]Danish Meteorological Institute, Copenhagen, Denmark
[8]Lamont-Doherty Earth Observatory, Columbia University, Palisades, NY, USA
[9]NASA Goddard Institute for Space Studies, New York, NY, USA
[10]Department of Geography and Earth Research Institute, University of California, Santa Barbara, Santa Barbara, CA, USA
[11]Nansen Environmental and Remote Sensing Center, Bergen, Norway
[12]Department of Environmental Sciences, Western Norway University of Applied Sciences, Sogndal, Norway
[13]Geophysical Institute, University of Bergen, Norway
[14]Antarctic and Sub-Antarctic Program, Universidad de Magallanes, Punta Arenas, Chile

Submitted on 3 April 2020 to ***International Journal of Climatology***

Revision submitted on 4 September 2020

This article has been accepted for publication and undergone full peer review but has not been through the copyediting, typesetting, pagination and proofreading process which may lead to differences between this version and the Version of Record. Please cite this article as doi: 10.1002/joc.6879

Keywords: air temperatures, Greenland, Greenland Blocking Index, sea ice

Abstract

Substantial marine, terrestrial, and atmospheric changes have occurred over the Greenland region during the last century. Several studies have documented record-levels of Greenland Ice Sheet (GrIS) summer melt extent during the 2000s and 2010s, but relatively little work has been carried out to assess regional climatic changes in other seasons. Here, we focus on the less studied cold-season (i.e., autumn and winter) climate, tracing the long-term (1873–2013) variability of Greenland's air temperatures through analyses of coastal observations and model-derived outlet glacier series and their linkages with North Atlantic sea ice, sea surface temperature (SST), and atmospheric circulation indices. Through a statistical framework, large amounts of west and south Greenland temperature variance (up to r^2~50%) can be explained by the seasonally-contemporaneous combination of the Greenland Blocking Index (GBI) and the North Atlantic Oscillation (NAO; hereafter the combination of GBI and NAO is termed GBI). Lagged and concomitant regional sea-ice concentration (SIC) and the Atlantic Multidecadal Oscillation (AMO) seasonal indices account for small amounts of residual air temperature variance (r^2<~10%) relative to the GBI. The correlations between GBI and cold-season temperatures are predominantly positive and statistically-significant through time, while regional SIC conditions emerge as a significant covariate from the mid-20th century through the conclusion of the study

period. The inclusion of the cold-season Pacific Decadal Oscillation (PDO) in multivariate analyses bolsters the air temperature variance explained by the North Atlantic regional predictors, suggesting the remote, background climate state is important to long-term Greenland temperature variability. These findings imply that large-scale tropospheric circulation has a strong control on surface temperature over Greenland through dynamic and thermodynamic impacts and stress the importance of understanding the evolving two-way linkages between the North Atlantic marine and atmospheric environment in order to more accurately predict Greenland seasonal climate variability and change through the 21st century.

1. Introduction

The North Atlantic has warmed over the last century with striking recent changes observed in its (sub)Arctic sector including GrIS melt extremes, loss of sea ice, cooling of the SSTs in the subpolar gyre, and persistent atmospheric circulation regimes (e.g., Straneo and Heimbach, 2013; Rahmstorf et al., 2015; Robson et al., 2018). Climate change impacts on the GrIS have received special attention due to the ice sheet's rapid response to atmospheric dynamical changes and warming, particularly since the 1980s (Tedesco et al., 2016; Mouginot et al., 2019; Hanna et al., 2020a; Shepherd et al., 2020). For example, outlet glacier retreat in southeast, central-west, and northwest Greenland more than tripled from 1992–2010 (Carr et al., 2017), while surface meltwater runoff over the last three decades has increased by nearly 40% (van den Broeke et al., 2017). During this period, warming-induced Greenland ice losses were enhanced by more frequent high-pressure blocking over the ice sheet associated with increases in the GBI (Hanna et al., 2016; van den Broeke et al., 2017; Pattyn et al., 2018; Noël et al., 2019).

At the intersection of Greenland glaciological and climatic research, connections have been drawn between observational/instrumental records, such as those spanning the 18th century to present that are curated by the Danish Meteorological Institute (DMI; Cappelen, 2020), and GrIS surface climate and processes. This has included the development and interpretation of statistically-downscaled (e.g., Box et al., 2009; Hanna et al., 2011) and regional climate model (e.g., Lenaerts et al., 2019; Mouginot et al., 2019) reconstructions of surface air temperature and ice sheet mass balance. Within this context, patterns and fluctuations in the coastal observations

can provide proxies for the ice sheet's seasonal climate and mass changes as well as response indicators to regional and global forcing.

Coastal Greenland air temperature analyses have largely centered on either identifying trends, often with emphasis on the summer melt season, or placing the recent multidecadal warming pattern in historical context, such as against the early 20th century warm period (Hanna et al., 2012; Mernild et al., 2014; Abermann et al., 2017, Hanna et al., 2020b). Much less attention has been paid to Greenland's autumn and winter temperature variability and identifying linkages and driving factors between the multidecadal temperature patterns and contemporaneous and lagged North Atlantic boundary (i.e., sea ice and SST) and atmospheric conditions. However, Hanna et al. (2013) analyzed links between Greenland weather station surface air temperatures and atmospheric and oceanic circulation indices for summer, finding some significant but spatially and temporally variable statistical associations between the air temperatures and the AMO, NAO, and GBI.

Greenland outlet glacier changes have also been linked to summer air temperature variability (Bevan et al., 2012; Khan et al., 2014; Carr et al., 2017) with limited consideration of the roles of autumn and winter temperatures. However, previous work has demonstrated that outlet glacier velocities increase gradually during winter, as the subglacial hydrological system repressures (Nienow et al., 2017). Furthermore, summers with high melt rates can lead to lower ice velocities in the subsequent winter: high summer melt causes the basal hydrology of the glacier to evolve into an efficient system earlier in the melt season and once this occurs, the impact of

additional meltwater inputs on ice velocities is more limited (Sole et al., 2013; Tedstone et al. 2013; 2015). Thus, ice velocities may be slower during warmer summers, due to the related drop in winter velocities. This highlights the importance of monitoring glacier change during the winter and assessing its relationship to both winter conditions and those in the previous summer. The seasonal formation of ice mélange (a temporary ice tongue made of icebergs held together by sea ice) at the front of ocean-terminating outlet glaciers is also thought to impact their discharge and frontal position: if the mélange forms earlier in the year, it may suppress calving and reduce terminus retreat, whereas later mélange formation allows for longer periods of high calving rates, facilitating glacier retreat (e.g., Sohn et al., 1998; Amundson et al., 2010; Carr et al., 2013; Moon et al., 2015). Finally, water can be stored both subglacially (Chu et al., 2016) and in firn aquifers over winter, with the latter being a potentially important, but often overlooked, component of Greenland's water and energy budget (Forster et al., 2014). Thus, limited evidence to date suggests that autumn and winter temperatures may influence snow cold content and glacier response to climate, but this has not been widely investigated.

Here we use a statistical framework to evaluate Greenland's long-term, cold-season (i.e., autumn and winter) coastal air temperature variability. We include model-derived, downscaled surface air temperatures for outlet glaciers proximate to these coastal sites in our analyses and compare the land versus glacial air temperature response to a common set of North Atlantic sea ice, SST, and atmospheric variables. We additionally compare the autumn and winter temperature series with frontal position data for selected outlet glaciers. To supplement these analyses, we test

a hypothesis, previously evaluated at the summer and annual timescales (e.g., Ding et al., 2014, 2019; Bonan and Blanchard-Wrigglesworth, 2020), that tropical/North Pacific teleconnections influence the North Atlantic ocean-atmosphere forcing of Greenland autumn and winter temperature variability.

2. Data and Methods

2.1 Analysis Periods and Seasonal Delineations

Analyses of Greenland coastal/glacial surface air temperatures from the standard two-meter (T2m) distance above the ground/ice surface are conducted for autumn (October–December; OND/au) and winter (January–March; JFM/wi) seasons. These seasonal definitions coincide with local changes and feedbacks involving the marine environment, namely following rapid sea ice formation and advance during OND and slower expansion and thickening in JFM as per marginal sea ice extent seasonal cycles (e.g., Peng and Meier, 2018). We note that the marginal seas in OND and JFM tend to not completely freeze over and exhibit some interannual variability, especially in regions overlapping the southern sea ice margin (**Table S1**).

Statistical analyses begin at the onset of the T2m observational records (1873, 1890, or 1895; **Table 1**) and conclude in 2013, which marks the final year of the Walsh et al (2015, 2017) sea ice dataset (described in Section 2.2). Oceanic and atmospheric predictor time series are selected, in part, because their records temporally overlap with the T2m data. Temperature analyses are conducted contemporaneously (lag-0) and also consider lagged associations over the prior two seasons (i.e., lag-1, lag-2).

2.2 Description of Air Temperature and Ocean-Ice-Atmosphere Indices

Monthly T2m time series, comprised of manual and automated observations, from five coastal locations, Upernavik (UPE; 04211), Ilulissat (ILU; 04221), Nuuk (NUK; 04250), Narsarsuaq/Ivittuut (NAR; 04270/34262), and Tasiilaq (TAS; 04360) were obtained from the Danish Meteorological Institute (DMI; Cappelen, 2014) (**Table 1)**. These datasets have undergone homogeneity testing and have been corrected against neighboring stations where appropriate resulting in T2m uncertainties of ~0.1°C (Cappelen, 2014). While some monthly coastal temperatures date back to 1784, we use only the more systematic set of long-term observations beginning in either 1873, 1890, or 1895. The records are >99% complete and missing months are filled using linear regression. The average of the five aforementioned station records also comprise the Composite Greenland Temperature 3 series that begins in 1895 (CGT3; Hanna et al., 2012).

Proximate to the DMI observations, monthly T2m series are reconstructed for five glaciers: Sermeq/Upernavik Isstrøm (SMQ), Sermeq Kujalleq/Jakobshavn Isbrae (SER), Kangiata Nunaata Sermia (KNS), Sermilik/Sermilik Brae (SMK), and Helheim Gletsjer (HEL) (**Table 1**). Surface air temperature data from Twentieth Century Reanalysis version 2 (20CRv2; Compo et al., 2011) and ERA-Interim Reanalysis (ERA-I; Dee et al., 2011) were downscaled and merged from their original horizontal resolutions to 5x5 km and topographically-adjusted using a digital elevation model and empirical ice-sheet lapse rates as described in Hanna et al (2005, 2011). Downscaled 20CRv2 T2m series from 1873-2008 were derived from Hanna et al (2011) and the ERA-I time series were similarly downscaled and then homogenized with the 20CRv2 product for the 1979–

2008 overlapping period to extend the temperature records to 2013. Long-term monthly air temperature comparisons between similarly downscaled model and station observations at Nuuk and Tasiilaq show strong agreement (see Figure 5a,b in Hanna et al., 2005), lending confidence in the downscaled product to capture near-coastal T2m variability. Glacier T2m, found 0-207 m asl (**Table 1**), is derived at the latitude and longitude centroid within each glacier's outlined polygon as identified by the Randolph Glacier Inventory (Pfeffer et al., 2014). These grid points are located in the lower ablation zone within ~50–110 km of the nearest DMI sites (**Table 1**). Analogous to the CGT3 time series, a composite glacier temperature (CGLT) record is created from the downscaled and aggregated seasonal glacier T2m values. We additionally compare variations in the HadCRUT4 (HAD) Northern Hemisphere near-surface air temperatures (Morice et al., 2012) against the glacier and coastal temperatures.

For three glaciers, SMQ, SER, and KNS, we analyze their long-term frontal position records in relation to their downscaled and nearby coastal temperatures. The frontal position series were constructed predominantly from satellite imagery, but also from evidence of Little Ice Age moraines. Full details of the frontal position reconstructions are provided in the following manuscripts: SMQ (Kahn et al., 2013; Andersen et al., 2014), SER (Steiger et al., 2018), and KNS (Lea et al., 2014). In all cases, frontal positions are relative to the last date of the series.

Regional (i.e., local) climate indices that describe the prevailing North Atlantic atmospheric circulation patterns are included in the analyses and referenced in **Table 2** along with the sea ice and SST data described below. The GBI data, derived from 20CRv2c (Compo et al.,

2011), are obtained from NOAA ESRL PSD and describe the mean 500 hPa geopotential height field over Greenland and adjacent marine areas from 60º–80ºN, 20º–80ºW (Hanna et al., 2016; 2018). Preliminary analyses comparing GBI time series before 1948 constructed with 20CRv2c and the new 20CRv3 (Slivinski et al., 2019) exhibit minimal interannual difference and strong, positive, and statistically-significant correlations in winter and autumn months (not shown). The North Atlantic Oscillation (NAO), Scandinavian pattern (SCA), and East Atlantic pattern (EA) time series are from Comas-Bru and Hernández (hereafter CBH; CBH 2018a,b). These series are created by empirical orthogonal function analysis (EOF) performed on sea-level pressure fields from five separate atmospheric reanalyses, 20CRv2c, NCEP/NCAR Reanalysis version 1 (Kalnay et al., 1996), ERA-40 (Uppala et al., 2005), ERA-I, and ERA-20C (Poli et al., 2016), which are then composited where the data temporally overlap (see CBH 2018a for details). To maintain temporal consistency in the analyses, the summer monthly (JJA) EA indices are omitted as they begin in 1900. As there are concerns with the 20CR fields during the early part of the record (e.g., CBH 2018a), we briefly assess the CBH NAO against the Hurrell NAO station-based index defined as the normalized sea-level pressure (SLP) difference between Ponta Delgada, Azores and Stykkisholmur/Reykjavik, Iceland (Hurrell, 1995). Running correlations presented in **Figure S1** show strong, positive, and statistically-significant seasonal covariance between these NAO indices for relevant seasons ($r>0.65$ in OND and $r>0.85$ in JFM). This result suggests that the CBH series generally capture temporal fluctuations in the observed North Atlantic pressure gradient.

Monthly sea-ice concentration (SIC; %) data on a 0.25ºx0.25º latitude-longitude grid are obtained from National Snow and Ice Data Center (Walsh et al., 2015; 2017). Version 1.1 of the reconstructed SIC product terminates in 2013, thereby marking our final analysis year. Grid cells are spatially-averaged for standard marginal sea domains proximate to Greenland (**Figure 1**), including the Canadian Archipelago (CAA), Hudson Bay (HUD), Baffin Bay (BAF), Labrador Sea (LAB), Greenland Sea (GRE), Iceland Sea (ICE), and Irminger Sea (IRM) for autumn and winter seasons.

To extend marginal sea analyses for retrospective spring and summer seasons categorized by partial to complete open water development, SSTs are obtained for the same marginal SIC domains. AMJ and JAS SSTs are selected from the Hadley Centre Global Sea Ice and Sea Surface Temperature (HadISST) dataset version 1.1 (Rayner et al., 2003). The monthly SST data are acquired at their native 1ºx1º degree grid and averaged to area-weighted seasonal values over the marginal SIC domains. To provide a more expansive perspective on North Atlantic SSTs, monthly, unsmoothed AMO (Enfield et al., 2001) time series are obtained from NOAA ESRL PSD.

In our analysis of Pacific climate forcing on Greenland autumn and winter T2m, we incorporate Niño 3.4 region (Trenberth, 1997) and PDO (Mantua et al., 1997) time series. The Niño 3.4 SST index, from NOAA ESRL PSD, is based on area-averaged HadISST1.1 data from 5ºN–5ºS and 170–120ºW. The PDO index, obtained from NOAA National Centers for Environmental Information, is based on an areally-averaged anomaly map that is created by

regressing the NOAA extended reconstruction of SST (ERSST version 4; Huang et al., 2014) anomalies against the Mantua PDO index over the North Pacific Ocean.

2.3 Statistical Framework

To assess aspects of temperature variability with time, standard deviations are calculated on the T2m data for select climatological periods and over the duration of the time series by applying 3 and 11-year centered approaches. Aside from standard deviation analyses of the raw temperatures, all climatic time series are normalized by the mean and standard deviation of the 1951–2000 period, then linearly detrended over the full length of the T2m records to emphasize interannual relationships.

A similar principal component-regression approach to Ballinger and Rogers (2014) is used to evaluate relationships between the ocean-ice-atmosphere series and the Greenland air temperature records. To avoid inflated variance in the regression model due to multicollinearity between highly correlated North Atlantic atmospheric circulation indices such as GBI and NAO (e.g., $r<-0.80$ for January, February, and March; Hanna et al., 2016), and to reduce the number of independent variables to a more interpretable predictor set, the seasonal indices (at 0, 1, and 2 season lags) are subjected to varimax rotated principal component analysis (PCA) to produce orthogonal, uncorrelated time series. Six separate PCAs are conducted following the first year of the station records (1873, 1890, or 1895) and respective season (autumn or winter). Across each analysis, rotated principal components (i.e., PCs) with eigenvalues >1 are retained, and these PCs cumulatively explain ≥73% of the variance of the original datasets. Each PC is given an

abbreviated name based on the seasonal index or indices that have ≥50% of their variance loaded onto that PC (see **Tables S2–S7**).

The PC time series, or scores, are subsequently used as orthogonal predictor variables in regression analyses aimed at hindcasting the long-term variability of the Greenland coastal and glacial T2m predictands. A stepwise multiple linear regression (SMLR) model is used here, which applies a forward selection procedure that begins by selecting the PC variable that explains the most T2m variance. The SMLR continues to enter and retain PC variables if they explain statistically-significant ($p \leq 0.05$) predictand variance. As the model iterates, adjusting sequentially for n-1 degrees of freedom, the total explained variance (r^2) cumulatively increases until significant predictors are no longer identified. The null hypothesis is that the PC predictors are not related to the T2m predictands such that the predictor coefficients are zero, which is rejected in the event PC(s) are retained by each SMLR model. The F-ratio determines global model significance, evaluating the probability that the null hypothesis is true across the model, while the significance of the individual PC predictors is evaluated with a two-tailed t-test.

The temporal variability and (in)stability of select, significant predictand-predictor relationships from the SMLR is further evaluated through running 30-year detrended Pearson's correlations. Wavelet coherence (Torrence and Compo, 1998; Grinsted et al., 2004) is also applied to assess strong bivariate relations involving air temperatures and their predictors as this method identifies covarying periodicities common amongst the time series. Statistical significance is

calculated using a Monte Carlo approach (Grinsted et al., 2004). Additional statistical analyses are described in the context of results.

3. Results

3.1 Air temperature variability and outlet glacier implications

Standard deviations of the T2m series are assessed for select periods in **Table 3**. The west coast sites and composited temperature indices commonly show the highest variability in analyses starting in either 1981 or 1991 with notably higher temperature spread in the winter versus autumn months and higher magnitudes for the coastal compared to the glacial sites. The largest standard deviations are found at UPE, NUK, and CGT3 during both seasons over the 1981–2010 period, while ILU (σ=4.95) and NAR (σ=3.76) saw the highest winter values over the same period. The HAD series similarly show the highest autumn and winter variability during 1981–2010, though with much smaller values compared to the land and glacial sites. From 1991–2013, the glacier air temperature variability in both seasons increased as the highest values occurred at SER, SMK, KNS, and HEL (tied with autumn 1901–1930), and for the CGLT series.

Higher variability at the coastal stations versus the glacier sites is apparent when comparing the running 3 and 11-year standard deviation plots in **Figure 2a,c** and **Figure 2b,d**. Increased temperature variability is notable in the autumn period from 1900 to 1920, then is consistently between 1.5 and 3σ for the west Greenland stations from the 1980s onward (**Figure 2a**). Autumn glacier temperatures exhibit a decrease from the late 1800s to early 1900s, then variability increases much like the nearby coastal sites from the 1900 to 1920 period with consistent (sub-)

decadal temperature fluctuations (**Figure 2b**). There are some sub-decadal extremes seen at the winter coastal stations in the late 18th century and between 1910 and 1920, but overall the decadal patterns from the 11-year running standard deviations suggest decreasing variability until roughly 1955, followed by a strong increase in variability to the mid-1980s at the west coast locations (to ~4–6σ; **Figure 2c**). Highly variable values during the 1981–2010 period capture these patterns (**Table 3**). The standard deviations slightly decrease thereafter, although they show decadal signatures that are comparable in magnitude to earlier periods (1890s and 1910s) before leveling off around 2000. Winter glacier temperature variability is relatively consistent, fluctuating around 1.5–2.5σ, until the early 2000s when the decadal variability tends to rise above previous years (**Figure 2d**), hence the high 1991–2013 period values previously discussed (**Table 3**).

As mentioned in Section 1, increasing cold-season air temperature variability and higher winter temperatures have several implications for Greenland's near-coastal environments. Focusing on autumn (OND) temperatures, no clear trend is apparent during the 1990s and 2000s (**Figure 3**). However, peak autumn T2m glacier air temperatures for the entire time series occurred during the 2000s, namely in 2009 at UPE (4.2σ above the 1951–2000 mean), in 2010 at SER (4.6σ), and KNS (3.7σ; **Figure 3**). Furthermore, autumn T2m temperature variability was highest at all locations except SMQ during the period 1991-2013 (**Table 3**). Higher absolute temperatures and higher temperature variability (**Table 3)** in the winter months ($r>0.99$, $p<0.05$ for raw versus detrended JFM T2m from 1991–2013) could impact terminus retreat rates. Thus, we compare winter temperatures and their variability to the long-term terminus positions for select glaciers

located proximal to meteorological stations with long-term records. Recent positive trends in winter temperatures from the mid-1990s (SMQ and KNS) and from ~2000 (SER) coincided with strong glacier retreat until the end of the study period (**Figure 3**). The period from 1991–2013 was also characterized by enhanced winter air temperature variability at the glaciers (**Table 3**; **Figure 3**). At UPE and SER, an earlier period of sustained retreat occurred between the mid-1930s and late 1950s, which coincided with a series of above-average winter temperatures (**Figure 3**). Taken together, this evidence suggests a correspondence and potential preconditioning effect of winter temperature trends and variability on subsequent glacier frontal position. The relationship to autumn temperatures is less clear, although our data suggest that enhanced autumn variability may coincide with recent rapid retreat (**Figure 3**; **Table 3**). While this analysis implicates cold-season air temperature effects on glacier termini, preceding summer air temperatures and melt processes are also known to play an important role in driving terminus changes (e.g., Catania et al., 2020).

3.2 Local predictive modes of air temperature changes

We holistically examine regional marine and atmospheric variables related to the Greenland long-term cold-season air temperature variations through multiple regression analyses. Along the x-axis of each plot in **Figures 4-5**, the predictor components are listed sequentially based on their respective PCA and follow the abbreviations provided in **Tables S2–S7**. West coast and south Greenland coastal and ice areas in autumn have at least 40% of their long-term T2m variance explained by the predictor sets (**Figure 4a–d**). Glacial T2m at these four sites shows a consistent

total variance range (r^2=59–67%) compared to the wider spread of the land sites (r^2=42–58%). In terms of the local glacier-land station pairs, with the exception of NUK relative to KNS (3% less explained variance), the predictors explain at least 13% more variance in the ablation areas versus the coastal tundra sites. This relationship is flipped on the east coast where predictor-explained TAS variance exceeds that of HEL by 13%.

Across the south/west sites and composite records (**Figures 4a–d,f**), the primary predictor accounting for most of the total variance in each regression model is the autumn GBI-NAO component (GBI_{au}). Variations in this atmospheric circulation component explain 21–40% of the overall station variance and ~46–49% of the glacier temperature variability with smaller amounts of variance consistently accounted for by positive correlation with the AMO autumn, summer, spring component ($AMO_{au,su,sp}$) and an anticorrelation with the BAF, CAA, HUD, LAB autumn SIC component (BAF-I_{au}; $r^2 \leq 12\%$; **Figures 4a–d**). In contrast, TAS autumn T2m is predominately explained by the $AMO_{au,su,sp}$ component (r^2=17%) followed by small residual amounts of variance accounted for by BAF, CAA, HUD, and LAB autumn SIC component (BAF-I_{au}), GRE summer and spring SIC component (GRE-$S_{su,sp}$), and the SCA spring component (SCA_{sp}), while no single predictor explains more than 9% (i.e., GBI_{au}) of the variance at HEL (**Figure 4e**).

Similar to autumn results, the winter regression models show a distinct pattern of stronger local marine and atmospheric associations with air temperature on the island's west/south periphery. There is at least a 25% decrease in model-explained variance between the NUK and NAR (r^2 = 69% and 68%, respectively) and ILU and UPE to the north with only a 4% difference

between the latter two locations (**Figure 5a–d**). At these sites the predictor variables also more robustly explain the glacial versus the land T2m with an increase in cumulative model variance moving southward along the coast from SMQ (r^2=46%) to SMK (r^2=62%). Land versus glacier differences in the total winter variance tend to be much less compared to autumn analyses (within ±8%). For the east Greenland locations, the predictors cumulatively account for only a fraction of TAS and HEL temperature variability relative to the variance explained in the south/west sites (**Figure 5e**).

Much like the autumn regression analyses, the GBI-NAO winter component (GBI_{wi}) presents a robust and consistently strong association with the long-term winter air temperatures in the south and west of the island (**Figure 5a–d,f**). A wide range of seasonal variance is explained by this predictor at the south and west land sites as GBI_{wi} explains 26% of the UPE winter variance to 52% of the variance at NAR and SMK. At NUK, BAF and LAB winter SIC component (BAF-I_{wi}) represents the only site with double-digit explained predictor variance (r^2=11%) in addition to GBI (**Figure 5d**). Moreover, the BAF, CAA, HUD, and LAB autumn SIC component (BAF-I_{au}) at UPE, SMQ, ILU, and SER, the BAF-I_{wi} component at NUK and KNS, and the BAF autumn and winter, CAA autumn, HUD autumn, and LAB autumn and winter SIC component (BAF-$I_{au,wi}$) for HEL, CGT3, and CGLT explain the second-most winter T2m variance behind the GBI component (**Figure 5**). The $AMO_{wi,au,su}$ predictor explains the most variance of any single predictor at TAS (r^2=8%), while the GBI_{wi} component explains 14% of the variance at HEL with smaller residual contributions (**Figure 5e**). For autumn and winter analyses, the GBI component tends to have

positive and statistically-significant regression coefficients. While the magnitude of the regression coefficients for each equation are not listed, most (except for UPE autumn, b=0.47) exceed +0.50, and are particularly high at SMK and KNS (b≥+0.65 for autumn and winter). These findings suggest that the south/westernmost glacier air temperatures are particularly sensitive to long-term regional atmospheric circulation forcing as 1°C increases in land and glacier air temperatures are accompanied by a GBI change of at least 0.5σ.

While the interannual to interdecadal predictability of the regression models is not tested in depth, such as by iteratively running each model forward by one year from the beginning of their records or for select sub-periods as with the standard deviation analyses in Section 3.1, a summary of model predictive skill is briefly described here as it relates to their residual time series. Of note, the residuals are relatively homoscedastic, fluctuating between ±1.5°C across the model, but show an even tighter dispersion during the eras of highest T2m variability: 1901–1930 and sub-periods from 1981 to 2013, where they are consistently between ±1°C. Averaged across the glacier and land air temperature models for these periods, the residual mean for the 1901–1930 period is 0.18°C during autumn and winter, while the 1981–2013 average is -0.04°C for autumn and -0.07°C for winter (not shown). Such small residuals during these periods suggest that year-to-year changes in the local variables, led by the GBI, reasonably account for multidecadal air temperature extremes around coastal Greenland.

3.3 Assessing the time-varying consistency of Greenland blocking on air temperature

Given the consistent appearance of the GBI component as a leading predictor in the long-term T2 models as shown in the previous section, we look to further isolate its seasonal covariability with T2m over the duration of their records. To assess (in)stability in the GBI-T2m multidecadal relationships, 30-year running detrended correlations are calculated for autumn and winter (**Figures 6-7**). These plots represent the end year of correlation analyses such that a coefficient in 2013, for example, reflects the correlation over the 1984–2013 period.

Substantial amounts of GBI predictor explained variance described in Section 3.2 are supported by the consistent, positive, and statistically-significant ($r>|0.36|$) autumn relationships between the GBI component and the majority of the T2m records (**Figure 6a**). Many of the correlations are strong ($r>0.70$) until 1910, during the middle portion of the records spanning roughly the 1950s to 1970s, and toward the end of study period (e.g., years spanning the late 1970s and early 1980s until the 2010s). KNS-GBI correlations are noticeably high throughout the record, especially for 30-year periods ending between 1925 and 1980 ($r\geq0.69$). NUK-GBI correlations are similarly strong ($r\geq0.64$) between 1940 and 1980. ILU-GBI correlations are insignificant for periods concluding between ~1910 and 1935, while UPE-GBI correlations also become insignificant between 1910 and 1945, before becoming consistently significant thereafter and conforming to a similar running correlation pattern as the other west/south sites. For periods ending in 1930-1965, HEL-GBI relationships are primarily significant and comparable in the 1940s to many of the south/west sites in terms of magnitude. For periods ending in 1950 to 1980, the HEL and TAS values decline, the latter switching phase and becoming anti-correlated with

GBI, consistent with the other T2m-GBI relations before exhibiting increased strength toward the end of the record.

Running correlations between winter T2m and GBI tend to be higher and more consistently significant across the data records than their autumn counterparts (**Figure 6b**). Aside from periods of insignificant correlations (e.g., UPE in the mid-1920s to mid-1930s and again during the 1970s and ILU in the 1920s and 1930s), the bivariate relationships are statistically significant across the south and west sites and tend to fluctuate between r=0.50 and r=0.80 at most locations. HEL and TAS relationships with the winter GBI component conversely show predominantly negative, insignificant correlations until becoming significant for years ending between the mid-1990s to early-2000s (e.g., HEL (TAS) $r \leq -0.42$ from 1996 (2001) to 2013). Notably, the CGT3 and CGLT covariability with GBI is consistently negative and overwhelmingly significant over of the analysis period. This is quite striking given that only TAS and HEL sites are negatively correlated with GBI, and the correlations with the south/west sites are consistently positive and above the significance threshold cutoff. Muted TAS and HEL T2m variability relative to the other sites (**Figure 2**; **Table 3**) and weak, long-term responses to GBI may represent factors strongly weighting the sign of the correlations involving composite temperatures and GBI.

While associations between GBI and T2m tend to be strong through time, the regression analyses in Section 3.2 also suggest that local sea-ice changes impact T2m variability. Moreover, the BAF SIC component is the most common secondary SMLR model predictor in both seasons (e.g., 2nd predictor in 7 (9) models of autumn (winter) T2m). Running correlations between

temperatures and the sea-ice reveal unstable and rather inconsistent relations through time. However, there is a strong, downward relationship characterized by negative and significant correlations, particularly in autumn, that emerges at several sites beginning in the early 1980s (**Figure 7**).

Despite consistency in the sign and broad statistical significance in the T2m and GBI correlations, there is some temporal variability in the coefficients' magnitudes, perhaps due to low frequency changes in the GBI as with the T2m data (Section 3.1), which is further investigated here through wavelet coherence analysis. Wavelet coherence is broadly in-phase throughout the plots. In autumn, the greatest coherence tends to be at periods of ≤8 years at the west/south sites notably around years beginning 1920, 1950, and 1980 (**Figure 8a–h**). An in-phase 16-year periodicity in common coherence is also noted in the composite temperature records that is roughly centered on 1940 and appears consistent in the glacier records between 1900 and 1980 (**Figure 8k,l**). In winter wavelet coherence analyses centered on 1920, there are some GBI-temperature associations at short periods (<4 years), otherwise a gap exists here in significant 4–8 year periodicities that corresponds to a time window of relatively weak running correlations (**Figure 9a–l**). Except at UPE, 16–32 year coherence is noted between 1920–1970 though these longer periodicities extend well into the cone of influence (COI), which is shown as semi-transparent in the figures. These results should be interpreted with caution due to the influence of edge effects (Grinsted et al., 2004; **Figure 9b–h,k,l**). HEL and TAS in both seasons differ from the other sites

and exhibit overall limited wavelet coherence with some sparse anti-phase associations in line with weak GBI-NAO forcing on the east relative to south/west coasts.

3.4 Do (extra)tropical Pacific teleconnections modify local forcing of air temperatures?

Given evidence of Pacific SST linkages with northeastern Canada and Greenland summer and annual air temperatures through regional atmospheric forcing (i.e., GBI/NAO; Ding et al., 2014, 2019; Bonan and Blanchard-Wrigglesworth, 2020), we evaluate whether (sub)tropical forcing modifies the local environmental and climate influences on Greenland cold-season T2m variability. We test for such relationships using similar methods as in Section 3.2; the PCA and SMLR models are re-run incorporating tropical Pacific indices (ENSO and/or PDO) and the total model-explained variance is then compared to that obtained by the local variables to determine the absolute change and thus the potential impact of (sub)tropical SSTs on the air temperatures (**Table 4**).

The addition of Niño 3.4 yields negligible change in autumn model explained variance (-4% at UPE to 0% for five sites including CGLT) except for CGT3 where total variance is reduced by 6%. The results are more substantial for winter as the inclusion of the Niño index decreases the explained variance across all sites (i.e., -1% at KNS to -10% at SMQ). Except for KNS, a more severe reduction in variance is noted for the glacier than land-based sites in the south/west areas. In contrast to Niño, the PDO index prompts an increase in model-explained autumn variance at over half the sites (n=7), particularly on the east coast where TAS and HEL variance increases by 8%. A similar number of sites observe variance increases by adding PDO winter to the model,

though the absolute changes are smaller at +1–3% relative to PDO autumn. The combined influence of Niño and PDO indices on T2m is also evaluated in similar fashion. Through the rotated PCA procedure, the concurrent and two preceding seasonal indices of each teleconnection tend to load onto their own component (e.g., $PDO_{wi,au,su}$ for the 1873-2013 regression analysis; not shown). Overall changes in explained variance are quite different between the autumn and winter regression model runs. For autumn, the variance increases at nine sites, including CGLT, ranging from 1% (several sites) to 4% at ILU. Meanwhile the winter changes are of opposite magnitude as the addition of both (sub)tropical indices yields a decline in variance at eight sites (from -2% at UPE and NAR to -5% at SMK) and no change at three others. None of the variance changes, however, are statistically significant (**Table 4)**.

Notably, the inclusion of PDO tends to bolster the predictability of Greenland T2m (**Table 4**). This occurs by increasing the variance of individual predictors common between the models that are run with and without (extra)tropical forcing (some examples include GBI and AMO components; but this analysis, which is analogous to Section 3.2, is not shown). Interestingly, the PDO component *is not* a consistent individual predictor of T2m within the models, suggesting instead that the total variance increases may be indirectly attributed to the North Pacific background climate state - as described in part by the PDO phase - which amplifies the local ice-ocean-atmosphere processes and feedbacks modulating Greenland coastal air temperatures.

4. Discussion

Our results indicate that autumn and winter North Atlantic Arctic atmospheric variability during the last century has a clear footprint in the long-term, cold-season Greenland air temperature records found along its south and west coast (i.e., UPE-SMQ, ILU-SER, NAR-SMK, and NUK-KNS). The consistency of the seasonally-contemporaneous Greenland blocking signal in the autumn and winter air temperatures is striking. When temporally deconstructed, the running correlation and wavelet analyses herein show that in-phase T2m-circulation coupling tends to be strongest over decadal periods of known extremes in both parameters within the early and middle 20th and late 20th/early 21st centuries. For instance, the decades of the 1960s and 2000s saw increased wintertime occurrence of warm air temperature extremes along west Greenland land areas (Mernild et al., 2014) and above-average incidence of anomalous Greenland blocking patterns (e.g., daily counts and seasonal mean values where GBI≥1σ; Hanna et al., 2015, 2018). Moreover, we find the winter air temperature response to overlying mid-tropospheric flow to more strongly project through time in the ablation areas versus terrestrial sites, notably at KNS and to a lesser extent at SER and SMQ to the north that may reflect an absence of marine effects further inland.

Our data demonstrate that accelerated terminus retreat at our study glaciers from the mid-1990s onwards coincided with a period of both higher and more variable winter air temperatures (**Figure 3**). The influence of winter air temperatures on Greenland outlet glacier retreat has not previously been assessed, but recent studies have highlighted the importance of winter ice motion for modulating interannual glacier velocities (e.g., Sole et al., 2013) and winter storage of

meltwater in firn (Forster et al., 2014) and at the glacier bed (Chu et al., 2016), hinting that winter conditions may be important for understanding Greenland's response to climate change. A detailed analysis of the potential mechanisms linking winter temperatures and glacier frontal position is beyond the scope of this paper and would require assessment at a broader number of study glaciers, to determine whether the relationship was pervasive. This should also be assessed in relation to air temperatures during the previous summer/spring, to determine the relative importance of air temperature changes in each season and the impact of antecedent conditions, which in turn would provide insight into the mechanisms by which air temperatures impact glacier frontal position. Here we offer a number of potential explanations for the observed relationship between frontal position and winter temperatures, which can be explored by future work. First, warmer and more variable winter temperatures could delay the formation of and/or result in a weaker ice mélange, which could in turn allow calving to continue later into the year and facilitate retreat (e.g., Sohn et al., 1998; Carr et al., 2013; Moon et al., 2015; Carr et al., 2017). Alternatively, higher temperatures in winter might result in increased water storage within firn layers (Forster et al., 2014) and/or crevasses, which could weaken near-terminus ice and facilitate increased calving, and hence glacier retreat. Finally, the sub-polar North Atlantic has warmed since the mid-1990s, which has been partly linked to changes in local atmospheric indices, and summer temperatures have also increased (e.g., Straneo and Heimbach, 2013). Thus, it may be that observed glacier retreat is a response to higher ocean temperatures and/or warmer summer air temperatures that have resulted from the same changes in the atmospheric conditions that are also driving higher and

more variable winter temperatures. With the available data, we cannot differentiate between these explanations, but the linkages between winter temperatures and glacier retreat warrants further investigation given the apparent correspondence between these variables (**Figure 3**; **Table 3**).

Regional ocean-atmosphere forcing tends to provide small residual predictability (r^2<~10%) relative to GBI, often from multiple-season AMO and lag-0 (-1) season BAF SIC autumn (winter) components (**Figures 3-4**). The small residual variance captured by these predictors over the period-long analyses does not preclude their multidecadal temperature influence. Instead, variations in BAF SIC components offer limited long-term predictability, but emerge around mid-century and couple with increased autumn and winter Greenland blocking events to regulate the west Greenland air temperatures (**Figures 6-7**). During the satellite-era, Ballinger et al (2018) corroborates these autumn (SOND) relationships, noting significant, bivariate detrended correlations between Baffin freeze onset dates and GBI and south/west Greenland coastal air temperatures (r=0.50–0.70 and 0.65–0.85, respectively). Recent (1990–2010) near-coastal 2Barrel (northwest Greenland) ice-core reconstructions by Osterberg et al (2015) identify an October and November Baffin SIC signal comparable to that found by Ballinger et al (2018) for clustered west coast sites between ~67–69°N. Through running correlation analyses, we show most south and west cold-season temperatures by the end of study period in 2013 are correlated with GBI at r>0.60 by 2013 (**Figure 6**), while most (several) autumn (winter) temperatures similarly show significant negative covariance with BAF SIC components beginning in the early 1980s and strengthening through time (**Figure 7**).

In contrast to the first half of the temperature records which encompass the early 20th century Arctic warm period, greater sensitivity of the coastal land and glacier ablation areas to atmospheric dynamics and to a lesser extent local sea ice conditions (represented through seasonal SIC) from the mid-20th century onward suggests the possible emergence of an open water-heat flux feedback that affects cold-season temperatures (**Figures 6-7**). The climatological ocean-to-atmosphere heat flux for the Baffin-Canadian Archipelago region increases with the magnitude of the vertical air temperature gradient from August to February (Screen, 2017). However, satellite-era lengthening of the region's melt season due to both earlier melt onset and later freeze-up (Stroeve and Notz, 2018) affects the timing and, depending on cloud conditions, can exacerbate the intensity of turbulent heat transfer to the overlying troposphere. Increases in the geopotential heights can ensue, supporting an anticyclonic circulation pattern that transports locally-derived sensible and latent heat onto the island's west coast. Another plausible link between the circulation anomalies and air temperatures is that periods of high GBI values tend to be characterized by a strong barotropic, tropospheric high-pressure anomaly over Greenland, which favors strong subsidence and adiabatic warming of the lower troposphere and surface (Rowley et al., 2019). The stronger correlation between Greenland T2m and GBI, compared to AMO and local sea ice, during autumn and winter suggests that surface temperature variability over Greenland in the cold season is more sensitive to the top-down atmospheric adiabatic processes rather than bottom-up ocean-driven change (Ding et al., 2014).

Potentially, a combination of these dynamic and thermodynamic processes play a role in contributing to the near-surface air temperature warming focused in the west/south edge of Greenland that is captured in both climate model and observationally-based analyses (Screen 2017; Ballinger et al., 2018; Pedersen and Christensen 2019). Of note, the local sea ice influence on air temperatures tends to be confined to low-elevation areas due to mesoscale wind features, such as katabatic flows, that frequently prevent the penetration of turbulent heat from the local marine environment upslope past the lower ablation zone (Ballinger et al., 2019). In addition to GBI and local oceanic mechanisms, atmospheric river frequency and intensity (Mattingly et al., 2018) and local storm activity (Lewis et al., 2019; Oltmanns et al., 2019) within the coastal areas represent a couple of the energy balance-related factors not explicitly integrated into our statistical models that likely contribute some residual temperature variance and precondition the ice sheet and peripheral glaciers for the subsequent melt season.

Additionally, statistical model iterations that include North Pacific SSTs (i.e., PDO) tend to amplify the regional ocean-atmosphere signals in the air temperatures. The influence of the PDO teleconnection manifests by increasing the total explained temperature variance often by inflating the GBI, AMO, and BAF SIC component predictors (not shown). The negative phase of the PDO, which occurs in 60% of autumn and 62% of winter seasons between 1873-2012, tends to produce a ~+0.5–1°C lower tropospheric winter (DJF) temperature anomaly pattern over Greenland (Screen and Francis, 2016). Under negative PDO, prevailing warm, southerly winds through the Pacific and Atlantic Arctic produce geopotential height increases through the depth of

the troposphere north of 70°N. The effects of the PDO background state combined with increased Rossby wave activity and affiliated moisture incursions into the Arctic since the early 1990s strongly influence cold-season sea ice loss and amplify the GBI through two-way ocean-atmosphere interactions (Gong et al., 2017; Hanna et al., 2018).

5. Conclusions

We identify a relatively sustained and statistically-significant connection between observed and model-downscaled Greenland autumn and winter air temperatures and the overlying, seasonally-concurrent blocking circulation pattern (i.e., GBI-NAO component). This pattern represents a primary, consistent control of air temperatures spanning Upernavik (UPE) to Narsarsuaq (NAR), with high predictability of glacier temperatures in the nearby ice sheet ablation zones ($r^2 \geq 37\%$). Contemporaneous and lagged Baffin sea ice conditions, and to a lesser extent AMO, play a smaller long-term role in temperature predictability, though emerge as significant covariates with air temperature in recent decades characterized by massive sea ice losses throughout the annual cycle. The addition of PDO enhances air temperature predictability over the long-term by increasing the variance of existing predictors (e.g., GBI, AMO, and BAF-I) likely through modulating Arctic air temperature-tropospheric pressure relations (e.g., negative PDO is linked with higher air temperatures and geopotential heights). Furthermore, our analyses demonstrate the coincidence between the onset of accelerated retreat from the mid-1990s at our study glaciers and both higher and more variable winter air temperatures which warrants further investigation. This was also a period of warmer summer temperatures, so further research is

required to determine the relative importance of the temperatures in different seasons and the mechanisms by which they drive glacier retreat, e.g. summer air temperatures may enhance melt, whilst winter air temperatures may impact sea ice conditions and hence buttressing on the glacier termini.

Beyond attribution of autumn and winter air temperature variability, there has been an increase in Greenland cold-season snow and glacial ice melt events due to weather extremes (Oltmanns et al., 2019). Despite a shift in the frequency distribution of thaw conditions against background climate warming, there is uncertainty as to what extent persistent cold-season local ocean-atmosphere conditions and associated snow accumulation and cold content development act as preconditioning factors for the subsequent spring/summer melt season. Therefore, continued efforts to monitor cold-season climate forcing and feedbacks related to Greenland surface air temperatures and their preparatory role in warm-season cryospheric processes may be important to attaining more complete understanding of the island's evolving coastal and ice sheet climate.

Acknowledgements

TJB acknowledges support from the University of Alaska Fairbanks Experimental Arctic Prediction Initiative. MT acknowledges support from the National Science Foundation (OPP19-01603), NASA (NNX17AH04G) and by the Heising-Simons Foundation (HS 2019 – 1160). We thank those who have made their data freely available online, and Anders Bjørk, Abbas Khan, Kristian Kjeldsen, James Lea, and Nadine Steiger for sharing the glacier frontal position datasets.

We thank three anonymous reviewers for offering critiques that have helped to improve the manuscript.

References

Abermann, J., Hansen, B., Lund, M., Wacker, S., Karami, M. and Cappelen, J. (2017) Hotspots and key periods of Greenland climate change during the past six decades. *Ambio*, 46, 3–11.

Amundson, J.M., Fahnestock, M., Truffer, M., Brown, J., Lüthi, M.P. and Motyka, R.J. (2010) Ice mélange dynamics and implications for terminus stability, Jakobshavn Isbræ, Greenland. *Journal of Geophysical Research: Earth Surface*, 115, doi:10.1029/2009JF001405,2010.

Andresen, C.S., Kjeldsen, K.K., Harden, B., Nørgaard-Pedersen, N. and Kjær, K.H. (2014) Outlet glacier dynamics and bathymetry at Upernavik Isstrøm and Upernavik Isfjord, north-west Greenland. *Geological Survey of Denmark and Greenland Bulletin*, 31, 79–82.

Ballinger, T.J. and Rogers, J.C. (2014) Climatic and atmospheric teleconnection indices and western Arctic sea ice variability. *Physical Geography*, 35, 459–477.

Ballinger, T.J., Hanna, E., Hall, R.J., Miller, J., Ribergaard, M.H. and Høyer, J.L. (2018) Greenland coastal air temperatures linked to Baffin Bay and Greenland Sea ice conditions during autumn through regional blocking patterns. *Climate Dynamics*, 50, 83–100.

Ballinger, T.J., Mote, T.L., Mattingly, K., Bliss, A.C., Hanna, E., van As, D., Prieto, M., Gharehchahi, S., Fettweis, X., Noël, B., Smeets, P.C.J.P., Reijmer, C.H., Ribergaard, M.H. and Cappelen, J. (2019) Greenland ice sheet late season melt: investigating multiscale drivers of K-transect events. *The Cryosphere*, 13, 2241–2257.

Bevan, S.L., Luckman, A.J., and Murray, T. (2012) Glacier dynamics over the last quarter century at Helheim, Kangerdlussuaq and 14 other major Greenland outlet glaciers. *The Cryosphere*, 6, 923–937.

Bjørk, A.A., Kruse, L.M. and Michaelsen, P.B. (2015) Brief communication: Getting Greenland's glaciers right – a new data set of all official Greenlandic glacier names. *The Cryosphere*, 9, 2215–2218.

Bonan, D.B. and Blanchard-Wrigglesworth, E. (2020) Nonstationary teleconnection between the Pacific Ocean and Arctic sea ice. *Geophysical Research Letters*, 47, doi:10.1029/2019GL085666.

Box, J.E., Yang, L., Bromwich, D.H. and Bai, L. (2009) Greenland ice sheet surface air temperature variability: 1840–2007. *Journal of Climate*, 22, 4029-4049.

Cappelen, J. (ed.) (2014) Greenland – DMI historical climate data collection 1784–2013. DMI Report 14-04, Danish Meteorological Institute, Copenhagen.

Cappelen, J. (ed.) (2020) Greenland – DMI historical data collection 1784–2019. DMI Report 20-04, Danish Meteorological Institute, Copenhagen.

Carr, J. R., Vieli, A. and Stokes, C.R. (2013) Climatic, oceanic and topographic controls on marine-terminating outlet glacier behavior in northwest Greenland at seasonal to interannual timescales. *Journal of Geophysical Research*, 118, 1210–1226.

Carr, J.R., Stokes, C.R. and Vieli, A. (2017) Threefold increase in marine-terminating outlet glacier retreat rates across the Atlantic Arctic: 1992–2010. *Annals of Glaciology*, 58, 72–91.

Catania, G.A., Stearns, L.A., Moon, T.A., Enderlin, E.M., and Jackson, R.H. (2020) Future evolution of Greenland's marine-terminating outlet glaciers. *Journal of Geophysical Research: Earth Surface*., 125, doi:10.1029/2018JF004873.

Chu, W., Schroeder, D.M., Seroussi, H., Creyts, T.T., Palmer, S.J. and Bell, R.E. (2016) Extensive winter subglacial water storage beneath the Greenland Ice Sheet. *Geophysical Research Letters*, 43, 12,484–12,492.

Comas-Bru, L. and Hernández, A. (2018a) Reconciling North Atlantic climate modes: revised monthly indices for the East Atlantic and the Scandinavian patterns beyond the 20th century. *Earth System Science Data*, 10, 2329–2344.

Comas-Bru, L. and Hernández, A. (2018b) (Dataset 2) Seasonal EOF-based indices of the North Atlantic Oscillation, the East Atlantic pattern, and the Scandinavia pattern covering the period from 1851 to present. PANGAEA, doi:10.1594/PANGAEA.892768. [Last Accessed 6 January 2020].

Compo, G.P., Whitaker, J.S., Sardeshmukh, P.D., Matsui, N., Allan, R.J., Yin, X., Gleason, B.E., Vose, R.S., Rutledge, G., Bessemoulin, P., Brönnimann, S., Brunet, M., Crouthamel, R.I., Grant, A.N., Groisman, P.Y., Jones, P.D., Kruk, M.C., Kruger, A.C., Marshall, G.J., Maugeri, M., Mok, H.Y., Nordli, 1., Ross, T.F., Trigo, R.M., Wang, X.L., Woodruff, S. D. and Worley, S.J. (2011) The twentieth century reanalysis project. *Quarterly Journal of the Royal Meteorological Society*, 137, 1–28.

Dee, D.P., Uppala, S.M., Simmons, A.J., Berrisford, P., Poli, P., Kobayashi, S., Andrae, U., Balmaseda, M.A., Balsamo, G., Bauer, P., Bechtold, P., Beljaars, A.C.M., van de Berg, L., Bidlot, J., Bormann, N., Delsol, C., Dragani, R., Fuentes, M., Geer, A.J., Haimberger, L., Healy, S.B., Hersbach, H., Hólm, E.V., Isaksen, L., Kållberg, P., Köhler, M., Matricardi, M., McNally, A.P., Monge-Sanz, B.M., Morcrette, J.-J., Park, B.K., Peubey, C., de Rosnay, P., Tavolato, C., Thépaut, J.-N. and Vitart, F. (2011) The ERA-Interim reanalysis: configuration and performance of the data assimilation system. *Quarterly Journal of the Royal Meteorological Society*, 137, 553–597.

Ding, Q., Wallace, J.M., Battisti, D.S., Steig, E.J., Gallant, A.J.E., Kim, H.-J. and Gei, L. (2014) Tropical forcing of the recent rapid Arctic warming in northeastern Canada and Greenland. *Nature*, 509, 209–212.

Ding, Q., Schweiger, A., L'Heureux, M., Steig, E.J., Battisti, D.S., Johnson, N.C., Blanchard-Wrigglesworth, E., Po-Chedley, S., Zhang, Q., Harnos, K., Bushuk, M., Markle, B. and Baxter, I. (2019) Fingerprints of internal drivers of Arctic sea ice loss in observations and model simulations. *Nature Geoscience*, 12, 28–33.

Enfield, D.B., Mestas-Nunez, A.M. and Trimble, P.J. (2001) The Atlantic Multidecadal Oscillation and its relationship to rainfall and river flows in the continental U.S. *Geophysical Research Letters*, 28, 2077–2080.

Forster, R.R., Box, J.E., van den Broeke, M.R., Miège, C., Burgess, E.W., van Angelen, J.H., Lenaerts, J.T., Koenig, L.S., Paden, J., Lewis, C. and Gogineni, S.P. (2014) Extensive liquid meltwater storage in firn within the Greenland ice sheet. *Nature Geoscience*, 7, 95–98.

Gong, T., Feldstein, S. and Lee, S. (2017) The role of downward infrared radiation in the recent Arctic winter warming trend. *Journal of Climate*, 30, 4937–4949.

Grinsted, A., Moore, J.C. and Jevrejeva, S. (2004) Application of the cross wavelet transform and wavelet coherence to geophysical time series. *Nonlinear Processes in Geophysics*, 11, 561–566.

Hanna, E., Huybrechts, P., Janssens, I., Cappelen, J., Steffen, K. and Stephens, A. (2005) Runoff and mass balance of the Greenland Ice Sheet: 1958–2003. *Journal of Geophysical Research Atmospheres*, 110, doi:10.1029/2004JD005641.

Hanna, E., Huybrechts, P., Cappelen, J., Steffen, K., Bales, R.C., Burgess, E., McConnell, J.R., Steffensen, J.P., van den Broeke, M., Wake, L., Bigg, G. and Savas, D. (2011) Greenland Ice Sheet surface mass balance 1870 to 2010 based on Twentieth Century Reanalysis, and links with global climate forcing. *Journal of Geophysical Research Atmospheres*, 116, doi:10. 1029/2011JD016387.

Hanna, E., Mernild, S.H., Cappelen, J. and Steffen, K. (2012) Recent warming in Greenland in a long-term instrumental (1881–2012) climatic context: I. Evaluation of surface air temperature records. *Environmental Research Letters*, 7, doi:10.1088/1748-9326/7/4/045404.

Hanna, E., Jones, J.M., Cappelen, J., Mernild, S.H., Wood, L., Steffen, K. and Huybrechts, P. (2013) The influence of North Atlantic atmospheric and oceanic forcing effects on 1900–2010 Greenland summer climate and ice melt/runoff. *International Journal of Climatology*, 33, 862-880.

Hanna, E., Cropper, T.E., Jones, P.D., Scaife, A.A. and Allan, R. (2015) Recent seasonal asymmetric changes in the NAO (a marked summer decline and increased winter variability) and associated changes in the AO and Greenland Blocking Index. *International Journal of Climatology*, 35, 2540–2554.

Hanna, E., Cropper, T.E., Hall, R.J. and Cappelen, J. (2016) Greenland Blocking Index 1851-2015: a regional climate change signal. *International Journal of Climatology*, 36, 4847-4861.

Hanna, E., Hall, R.J., Cropper, T.E., Ballinger, T.J., Wake, L., Mote, T. and Cappelen, J. (2018) Greenland blocking index daily series 1851–2015: Analysis of changes in extremes and links with North Atlantic and UK climate variability and change. *International Journal of Climatology*, 38, 3546–3564.

Hanna, E., Pattyn, F., Navarro, F., Favier, V., Goelzer, H., van den Broeke, M.R., Vizcaino, M., Whitehouse, P.L., Ritz, C., Bulthuis, K. and Smith, B. (2020a) Mass balance of the ice sheets and glaciers – Progress since AR5 and challenges. *Earth-Science Reviews*, 201, 1–17.

Hanna, E., Cappelen, J., Fettweis, X., Mernild, S.H., Mote, T.L., Mottram, R., Steffen, K., Ballinger, T.J. and Hall, R. (2020b) Greenland surface air temperature changes from 1981 to 2019 and implications for future ice-sheet melt and mass-balance change. *International Journal of Climatology*, doi:10.1002/joc.6771.

Huang, B., Banzon, V.F., Freeman, E. Lawrimore, J., Liu, W., Peterson, T.C., Smith, T.M., Thorne, P.W., Woodruff, S.D. and Zhang, H.-M. (2014) Extrended Reconstructed Sea Surface

Temperature version 4 (ERSST.v4). Part I: Upgrades and intercomparisons. *Journal of Climate*, 28, 911–930.

Hurrell, J.W. (1995) Decadal trends in the North Atlantic Oscillation: Regional temperatures and precipitation. *Science*, 269, 676–679.

Khan, S.A., Kjær, K.H., Korsgaard, N.J., Wahr, J., Joughin, I.R., Timm, L.H., Bamber, J.L., van den Broeke, M.R., Stearns, L.A., Hamilton, G.S. and Csatho, B.M. (2013) Recurring dynamically induced thinning during 1985 to 2010 on Upernavik Isstrøm, West Greenland. *Journal of Geophysical Research: Earth Surface*, 118, 111–121.

Kalnay, E., Kanamitsu, M., Kistler, R., Collins, W., Deaven, D., Gandin, L., Iredell, M., Saha, S., White, G., Woollen, J., Zhu, Y., Chelliah, M., Ebisuzaki, W., Higgins, W., Janowiak, J., Mo, K. C., Ropelewski, C., Wang, J., Leetmaa, A., Reynolds, R., Jenne, R. and Joseph, D. (1996) The NCEP/NCAR 40-Year Reanalysis Project. *Bulletin of the American Meteorological Society*, 77, 437–472.

Khan, S.A., Kjær, K.H., Bevis, M., Bamber, J.L., Wahr, J., Kjeldsen, K.K., Bjørk, A.A., Korsgaard, N.J., Stearns, L.A., van den Broeke, M.R., Liu, L., Larsen, N.K. and Muresan, I.S. (2014) Sustained mass loss of the northeast Greenland ice sheet triggered by regional warming. *Nature Climate Change*, 4, 292–299.

Lea, J.M., Mair, D.W.F., Nick, F.M., Rea, B.R., van As, D., Morlighem, M., Nienow, P.W. and Weidick, A. (2014) Fluctuations of a Greenlandic tidewater glacier driven by changes in atmospheric forcing: observations and modelling of Kangiata Nunaata Sermia, 1859–present. *The Cryosphere*, 8, 2031–2045.

Lenaerts, J.T.M., Medley, B., van den Broeke, M.R., and Wouters, B. (2019) Observing and modeling ice sheet surface mass balance. *Reviews of Geophysics*, 57, 376-420.

Lewis, G., Osterberg, E., Hawley, R., Marshall, H.P., Meehan, T., Graeter, K., McCarthy, F., Overly, T., Thundercloud, Z. and Ferris, D. (2019) Recent precipitation decrease across the western Greenland ice sheet percolation zone. *The Cryosphere*, 13, 2797–2815.

Mantua, N.J., Hare, S.R., Zhang, Y., Wallace, J.M. and Francis, R.C. (1997) A Pacific interdecadal climate oscillation with impacts on salmon production. *Bulletin of the American Meteorological Society*, 78, 1069–1080.

Mattingly, K.S., Mote, T.L. and Fettweis, X. (2018) Atmospheric river impacts on the Greenland ice sheet. *Journal of Geophysical Research: Atmospheres*, 123, 8538–8560.

Mernild, S.H., Hanna, E., Yde, J.C., Cappelen, J. and Malmros, J.K. (2014) Coastal Greenland air temperature extremes and trends 1890–2010: annual and monthly analysis. *International Journal of Climatology*, 34, 1472–1487.

Moon, T., Joughin, I. and Smith, B. (2015) Seasonal to multiyear variability of glacier surface velocity, terminus position, and sea ice/ice mélange in northwest Greenland. *Journal of Geophysical Research: Earth Surface*, 120, 818–833.

Morice, C.P., Kennedy, J.J., Rayner, N.A. and Jones, P.D. (2012) Quantifying uncertainties in global and regional temperature change using an ensemble of observational estimates: the HadCRUT4 dataset. *Journal of Geophysical Research*, 111, doi:10.1029/2011JD017187.

Morlighem, M., Williams, C.N., Rignot, E., An, L., Arndt, J.E., Bamber, J.L., Catania, G., Chauché, N., Dowdeswell, J.A., Dorschel, B., Fenty, I., Hogan, K., Howat, I., Hubbard, A., Jakobsson, M., Jordan, T.M., Kjeldsen, K.K., Millan, R., Mayer, L., Mouginot, J., Noël, B.P.Y., O'Cofaigh, C., Palmer, S., Rysgaard, S., Seroussi, H., Siegert, M.J., Slabon, P., Straneo, F., van den Broeke, M.R., Weinrebe, W., Wood, M. and Zinglersen, K.B. (2017) BedMachine v3: Complete bed topography and ocean bathymetry mapping of Greenland from multibeam echo sounding combined with mass conservation. *Geophysical Research Letters*, 44, 11051–11061.

Mouginot, J., Rignot, E., Bjørk, A.A., van den Broeke, M., Millan, R., Morlighem, M., Noël, B., Scheuchl, B. and Wood, M. (2019) Forty-six years of Greenland Ice Sheet mass balance from 1972 to 2018. *Proceedings of the National Academy of Sciences*, 116, 9239–9244.

Nienow, P., Sole, A., Slater, D. and Cowton, T. (2017) Recent Advances in Our Understanding of the Role of Meltwater in the Greenland Ice Sheet System. *Current Climate Change Reports*, 3, 330–344.

Noël, B., van de Berg, W.J., Lhermitte, S. and van den Broeke, M.R. (2019) Rapid ablation zone expansion amplifies north Greenland mass loss. *Science Advances*, 5, doi:10.1126/sciadv.aaw0123.

Oltmanns, M., Straneo, F. and Tedesco, M. (2019) Increased Greenland melt triggered by large-scale, year-round cyclonic moisture intrusions. *The Cryosphere*, 13, 815–825.

Osterberg, E.C., Hawley, R.L., Wong, G., Kopec, B., Ferris, D. and Howley, J. (2015) Coastal ice-core record of recent northwest Greenland temperature and sea-ice concentration. *Journal of Glaciology*, 61, 1137–1146.

Pattyn, F., Ritz, C., Hanna, E., Asay-Davis, X., DeConto, R., Durand, G., Favier, L., Fettweis, X., Goelzer, H., Golledge, N.R., Kuipers Munneke, P., Lenaerts, J.T.M., Nowicki, S., Payne, A.J., Robinson, A., Seroussi, H., Trusel, L.D. and van den Broeke, M. (2018) The Greenland and Antarctic ice sheets under 1.5°C global warming. *Nature Climate Change*, 8, 1053–1061.

Pedersen, R.A. and Christensen, J.H. (2019) Attributing Greenland warming patterns to regional Arctic sea ice loss. *Geophysical Research Letters*, 46, 10,495–10,503.

Peng, G., and W.N. Meier, 2018: Temporal and regional variability of Arctic sea-ice coverage from satellite data. *Annals of Glaciology*, 59, 191-200.

Pfeffer, W. T., Arendt, A. A., Bliss, A., Bolch, T., Cogley, J. G., Gardner, A. S., Hagen, J.-O., Hock, R., Kaser, G., Kienholz, C., Miles, E. S., Moholdt, G., Mölg, N., Paul, F., Radić, V., Rastner, P., Raup, B., Rich, J. and Sharp, M. J. (2014) The Randolph Glacier Inventory: a globally complete inventory of glaciers. *Journal of Glaciology*, 60, 537–552.

Poli, P., Hersbach, H., Dee, D. P., Berrisford, P., Simmons, A. J., Vitart, F., Laloyaux, P., Tan, D. G. H., Peubey, C., Thépaut, J.-N., Trémolet, Y., Hólm, E. V., Bonavita, M., Isaksen, L. and Fisher, M. (2016) ERA-20C: An Atmospheric Reanalysis of the Twentieth Century. *Journal of Climate*, 29, 4083–4097.

Rahmstorf, S., Box, J.E., Feulner, G., Mann, M.E., Robinson, A., Rutherford, S. and Schaffernicht, E.J. (2015) Exceptional twentieth-century slowdown in the Atlantic Ocean overturning circulation. *Nature Climate Change*, 5, 475–480.

Rayner, N.A., Parker, D.E., Horton, E.B., Folland, C.K., Alexander, L.V., Rowell, D.P., Kent, E.C. and Kaplan, A. (2003) Global analyses of sea surface temperature, sea ice, and night marine air temperature since the late nineteenth century. *Journal of Geophysical Research*, 108, doi:10.1029/2002JD002670.

Robson, J., Sutton, R.T., Archibald, A., Cooper, F., Christensen, M., Gray, L.J., Holliday, N.P. Macintosh, C., McMillan, M., Moat, B., Russo, M., Tilling, R., Carslaw, K., Desbruyéres, D., Embrey, O., Feltham, D.L., Grosvenor, D.P., Josey, S., King, B., Lewis, A., McCarthy, G.D., Merchant, C., New, A.L., O'Reily, C., Osprey, S.M., Read, K., Scaife, A., Shepherd, A., Sinha, B., Smeed, D., Smith, D., Ridout, A., Woollings, T. and Yang, M. (2018) Recent multivariate changes in the North Atlantic climate system with a focus on 2005–2016. *International Journal of Climatology*, 38, 5050–5076.

Rowley, N.A., A.M. Carleton, and J. Fegyveresi, 2019: Relationships of West Greenland supraglacial melt-lakes with local climate and regional atmospheric circulation. *International Journal of Climatology*, 40, 1164-1177.

Screen, J.A. and Francis, J.A. (2016) Contribution of sea-ice loss to Arctic amplification is regulated by Pacific Ocean decadal variability. *Nature Climate Change*, 6, 856–860.

Screen, J.A. (2017) Simulated atmospheric response to regional and pan-Arctic sea ice loss. *Journal of Climate*, 30, 3945–3962.

Shepherd, A. and the IMBIE Team (2020) Mass balance of the Greenland Ice sheet from 1992 to 2018. *Nature*, 579, 233–239.

Slivinski, L. C., G.P. Compo,, J.S. Whitaker, P.D. Sardeshmukh, B.S. Giese, C. McColl, R. Allan, X. Yin, R. Vose, H. Titchner, J. Kennedy, L.J. Spencer, L. Ashcroft, S. Brönnimann, M. Brunet, D. Camuffo, R. Cornes, T.A. Cram, R. Crouthamel, F. Domínguez-Ca stro, J.E. Freeman, J. Gergis, E. Hawkins, P.D. Jones, S. Jourdain, A. Kaplan, H. Kubota, F. Le Blancq, T. Lee, A. Lorrey, J. Luterbacher, M. Maugeri, C.J. Mock, G.W.K. Moore, R. Przybylak, C. Pudmenzky, C. Reason, V.C. Slonosky, C. Smith, B. Tinz, B. Trewin, M.A. Valente, X.L. Wang, C. Wilkinson, K. Wood, and P. Wyszyński, 2019: Towards a more reliable historical reanalysis: Improvements for version 3 of the Twentieth Century Reanalysis system. *Quarterly Journal of the Royal Meteorological Society*, 145, 2876-2908.

Sohn, H.G., Jezek, K.C. and van der Veen, C.J. (1998) Jakobshavn Glacier, west Greenland: 30 years of spaceborne observations. *Geophysical Research Letters*, 25, 2699–2702.

Sole, A., Nienow, P., Bartholomew, I., Mair, D., Cowton,T., Tedstone, A. and King, M. (2013) Winter motion mediates dynamic response of the Greenland Ice Sheet to warmer summers, *Geophysical Research Letters*, 40, 3940–3944.

Steiger, N., Nisancioglu, K.H., Åkesson, H., de Fleurian, B. and Nick, F.M. (2018) Simulated retreat of Jakobshavn Isbræ since the Little Ice Age controlled by geometry. *The Cryosphere*, 12, 2249–2266.

Straneo, F., and Heimbach, P. (2013) North Atlantic warming and the retreat of Greenland's outlet glaciers. *Nature*, 504, 36–43.

Stroeve, J. and Notz, D. (2018) Changing state of Arctic sea ice across all seasons. *Environmental Research Letters*, 13, doi:10.1088/1748-9326/aade56.

Tedesco, M., Mote, T., Fettweis, X., Hanna, E., Jeyaratnam, J., Booth, J.F., Datta, R. and Briggs, K. (2016) Arctic cut-off high drives the poleward shift of a new Greenland melting record. *Nature Communications*, 7, doi:10.1038/ncomms11723.

Tedstone, A.J., Nienow, P.W., Sole, A.J., Mair, D.W., Cowton, T.R., Bartholomew, I.D., and King, M.A. (2013) Greenland ice sheet motion insensitive to exceptional meltwater forcing. *Proceedings of the National Academy of Sciences*, 110, 19719-19724.

Tedstone, A.J., Nienow, P.W., Gourmelen, N., Dehecq, A., Goldberg, D., and Hanna, E. (2015) Decadal slowdown of a land-terminating sector of the Greenland Ice Sheet despite warming. *Nature*, 526, 692-695.

Torrence, C. and Compo, G.P. (1998) A practical guide to wavelet analysis. *Bulletin of the American Meteorological Society*, 79, 61–78.

Trenberth, K.E. (1997) The definition of El Niño. *Bulletin of the American Meteorological Society*, 78, 2771–2778.

van den Broeke, M., Box, J., Fettweis, X., Hanna, E., Noël, B., Tedesco, M., van As, D., van de Berg, W.J. and van Kampenhout, L. (2017) Greenland Ice Sheet surface mass loss: Recent developments in observation and modeling. *Current Climate Change Reports*, 3, 345–356.

Uppala, S. M., Kållberg, P. W., Simmons, A. J., Andrae, U., Da Costa Bechtold, V., Fiorino, M., Gibson, J.K., Haseler, J., Hernandez, A., Kelly, G. A., Li, X., Onogi, K., Saarinen, S., Sokka, N., Allan, R. P., Anderson, E., Arpe, K., Balmaseda, M. A., Beljaars, A. C. M., Van De Berg, L., Bidlot, J., Bormann, N., Caires, S., Chevallier, F., Dethof, A., Dragosavac, M., Fisher, M., Fuentes, M., Hagemann, S., Hólm, E., Hoskins, B. J., Isaksen, L., Janssen, P. A. E. M., Jenne, R., Mcnally, A. P., Mahfouf, J.-F., Morcrette, J.-J., Rayner, N. A., Saunders, R. W., Simon, P., Sterl, A., Trenbreth, K. E., Untch, A., Vasiljevic, D., Viterbo, P., and Woollen, J., 2005: The ERA-40 re-analysis. *Quarterly Journal of the Royal Meteorological Society*, 131, 2961–3012.

Walsh, J. E., Chapman, W.L. and Fetterer, F. (2015) Gridded Monthly Sea Ice Extent and Concentration, 1850 Onward, Version 1.1. Boulder, Colorado USA. NSIDC: National Snow and Ice Data Center. doi:10.7265/N5833PZ5. [Last Accessed 1 February 2019].

Walsh, J.E., Fetterer, F., Stewart, J.S. and Chapman, W.L. (2017) A database for depicting Arctic sea ice variations back to 1850. *Geographical Review*, 107, 89–107.

Tables

T2m Sites (WMO #)	Abbreviation	Elevation (m)	Distance to the coast/ nearest T2m land site (km)	Coordinates	Starting Year
Upernavik[l] (04211)	UPE	126	0.28	72.78°N, 56.13°W	1873
Sermeq/ Upernavik Isstrøm[g]	SMQ	120	10.95/61.11	72.84°N, 54.28°W	1873
Ilulissat[l] (04221)	ILU	29	1.58	69.23°N, 51.07°W	1873
Sermeq Kujalleq/ Jakobshavn Isbrae[g]	SER	0	14.49/50.93	69.18°N, 49.80°W	1873
Nuuk[l] (04250)	NUK	80	0.25	64.17°N, 51.75°W	1890
Kangiata Nunaata Sermia[g]	KNS	102	2.65/107.31	64.30°N, 49.61°W	1890
Narsarsuaq (04270)/ Ivittuut[l] (34262)	NAR	27	1.42	61.17°N, 45.42°W	1873
Sermilik/Sermilik Brae[g]	SMK	0	3.77/90.62	60.98°N, 46.99°W	1873
Tasiilaq[l] (04360)	TAS	53	1.06	65.60°N, 37.63°W	1895
Helheim Gletsjer[g]	HEL	207	6.50/92.78	66.37°N, 38.31°W	1895

Table 1 Manual/station-derived land and statistically-downscaled glacier two-meter air temperature (T2m) site details (Hanna et al., 2005; 2011; Cappelen, 2014, 2020). Greenland Ice Sheet (GrIS) naming conventions are listed as official name/foreign name where both exist following Bjork et al. (2015), otherwise only the official name is listed. Superscript classification indicates sites on land (l) or glaciers attached to the Greenland Ice Sheet (g). Glacier centroid coordinates follow Pfeffer et al (2014). Glacier centroid elevations are taken from the ice surface layer in BedMachine3 (Morlighem et al., 2017).

Regional Ocean-Ice-Atmosphere Indices	**Seasons**	**Source**
Canadian Archipelago (CAA), Hudson (HUD), Baffin (BAF); Labrador (LAB); Greenland (GRE); Iceland (ICE); Irminger (IRM) SST	AMJ, JAS	Rayner et al. (2003)
CAA, HUD, BAF, LAB, GRE, ICE, IRM SIC	JFM, OND	Walsh et al. (2017)
Greenland Blocking (GBI)	JFM, AMJ, JAS, OND	Hanna et al. (2016)
North Atlantic Oscillation (NAO)	JFM, AMJ, JAS, OND	Comas-Bru and Hernández (2018)
East Atlantic Pattern (EA)	JFM, OND	Comas-Bru and Hernández (2018)
Scandinavian Pattern (SCA)	JFM, AMJ, JAS, OND	Comas-Bru and Hernández (2018)
Atlantic Multidecadal Oscillation (AMO)	JFM, AMJ, JAS, OND	Enfield et al. (2001)

Table 2 The list of North Atlantic ocean-ice-atmosphere indices, reduced through principal components analysis, and then used in multiple regression analyses. Seasons of index use in the statistical analyses and their sources are also shown. Autumn (OND) air temperatures are regressed against contemporaneous (OND) and previous summer (JAS) and spring (AMJ) indices, while winter (JFM) air temperatures are regressed against JFM and lagged OND and JAS indices.

Site	Season	Full Period	1901–1930	1921–1950	1941–1970	1961–1990	1981–2010	1991–2013
UPE	OND	2.34	*2.29*	1.56	1.87	2.04	**2.50**	2.04
	JFM	3.62	*3.78*	3.66	2.82	3.68	**3.99**	3.51
SMQ	OND	1.53	1.02	1.29	1.43	1.48	**1.88**	*1.85*
	JFM	2.06	1.62	1.85	1.97	2.21	*2.41*	**2.51**
ILU	OND	1.91	**1.93**	1.62	1.65	1.58	*1.73*	1.55
	JFM	4.18	4.19	3.47	2.89	*4.44*	**4.95**	4.20
SER	OND	1.56	1.23	1.29	1.61	1.48	*1.87*	**1.94**
	JFM	2.01	1.78	1.80	1.77	2.05	*2.75*	**2.97**
NAR	OND	1.80	1.49	1.60	1.68	1.78	*2.05*	**2.14**
	JFM	2.83	2.41	2.25	1.53	*3.68*	**3.76**	3.15
SMK	OND	1.20	0.81	0.88	1.10	1.03	*1.58*	**1.75**
	JFM	1.43	1.20	1.27	1.02	1.36	*2.06*	**2.31**
NUK	OND	1.47	1.42	1.25	1.41	1.23	**1.57**	*1.45*
	JFM	2.50	2.36	2.23	1.75	*2.97*	**3.13**	2.57
KNS	OND	1.56	1.21	1.38	1.65	1.50	*1.78*	**1.87**
	JFM	2.03	1.91	1.90	1.69	2.09	*2.54*	**2.55**
TAS	OND	1.47	**1.52**	1.20	*1.38*	1.16	1.23	1.07
	JFM	2.09	**2.54**	1.76	1.72	1.97	*2.01*	1.72
HEL	OND	1.27	**1.31**	1.25	1.18	1.27	1.28	**1.31**
	JFM	1.44	1.38	1.41	1.35	1.45	*1.63*	**1.71**
CGT3	OND	1.53	1.50	1.25	1.35	1.28	**1.63**	*1.52*
	JFM	2.75	2.79	2.36	1.73	*3.00*	**3.39**	2.88
CGLT	OND	1.27	1.01	1.08	1.25	1.20	*1.54*	**1.60**
	JFM	1.69	1.53	1.51	1.42	1.68	*2.14*	**2.25**
HAD	OND	0.39	0.22	0.21	0.19	*0.25*	**0.28**	0.19
	JFM	0.35	0.20	0.15	0.15	0.19	**0.31**	*0.26*

Table 3 Standard deviations (σ) of T2m autumn (OND) and winter (JFM) for the full study period (1873–2013) and select sub-periods. The highest sub-period σ values for each location are shown in **bold** and second highest are shown in *italics*. Global T2m from HADCRUT4 (HAD) are also included for comparison.

Location	Niño 3.4 OND Δr^2	Niño 3.4 JFM Δr^2	PDO OND Δr^2	PDO JFM Δr^2	Niño 3.4 & PDO OND Δr^2	Niño 3.4 & PDO JFM Δr^2
UPE	-4	-3	+3	+3	+1	-2
SMQ	-1	-10	+1	-1	+1	-4
ILU	-1	-4	+4	+2	+4	-3
SER	-3	-6	-1	+1	+1	-3
NAR	-1	-5	+2	+2	+2	-2
SMK	0	-7	-1	0	+3	-5
NUK	-2	-4	0	-1	-2	-3
KNS	0	-1	0	0	+1	-3
TAS	0	-4	+8	+1	+4	0
HEL	0	-4	+8	+3	+1	0
CGT3	-6	-3	-2	+3	-2	+3
CGLT	0	-4	+1	+3	-2	0

Table 4 Absolute change in the SMLR explained variance (%) between models with only local North Atlantic predictors (here referenced as NAT, as shown in **Figures 4** and **5**) and models that also include one or both Pacific climate indices (e.g., $SMLR_{NATL+PDO}$ r^2 *minus* $SMLR_{NATL}$ r^2). An F-test is applied under the null hypothesis that the residuals produced from these disparate model runs have equal variance. Across all of these tests, we fail to reject the null hypothesis of equal variance, indicating there are not statistically significant ($p \leq 0.05$) residual differences between the models with and without Pacific climate indices.

Figures

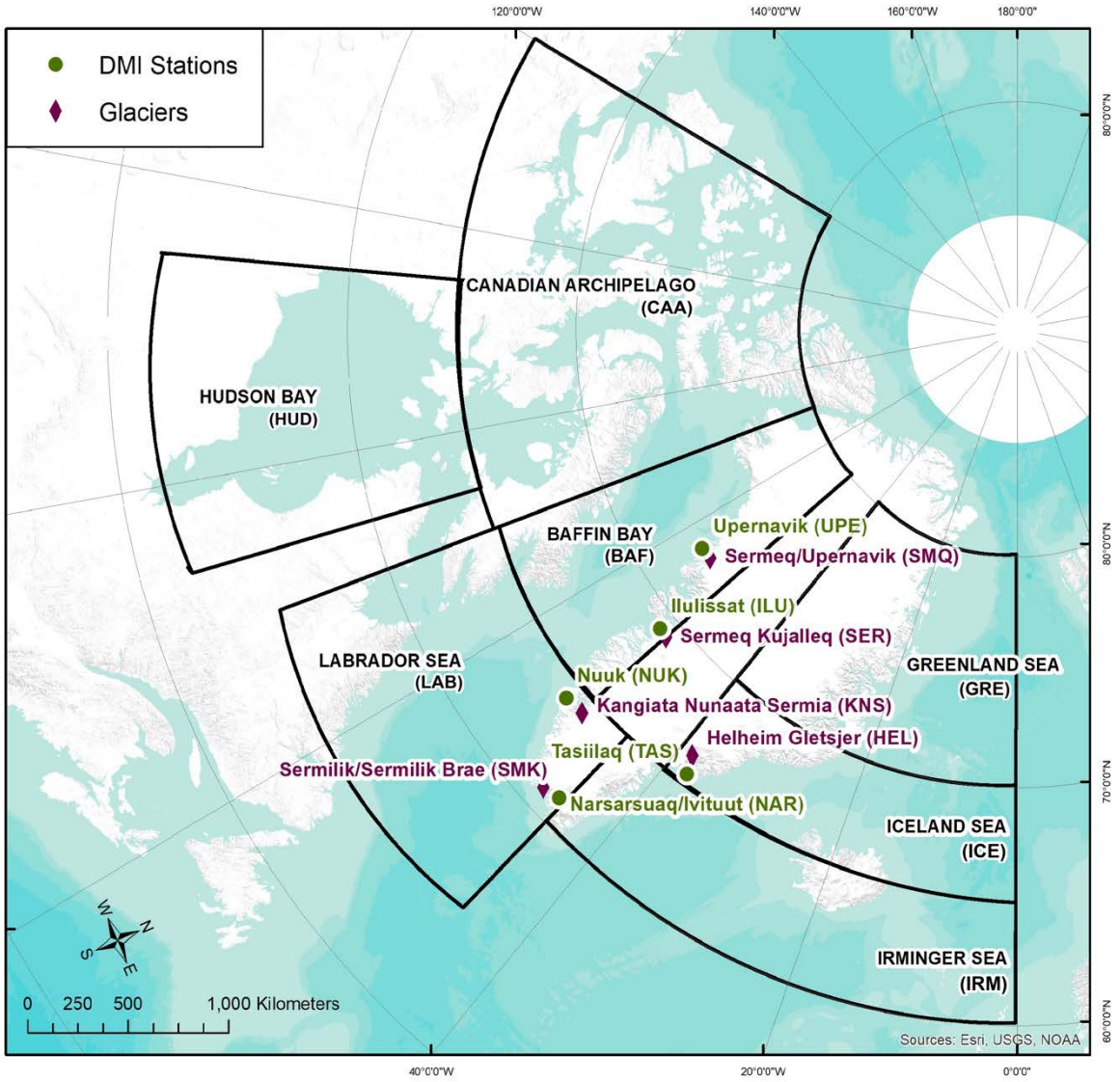

Figure 1 Study area map with circles (diamonds) marking the Greenland coastal (outlet glacier positions) where T2m measurements are obtained. Black polygons outline the marginal SIC and SST regions used in the analysis.

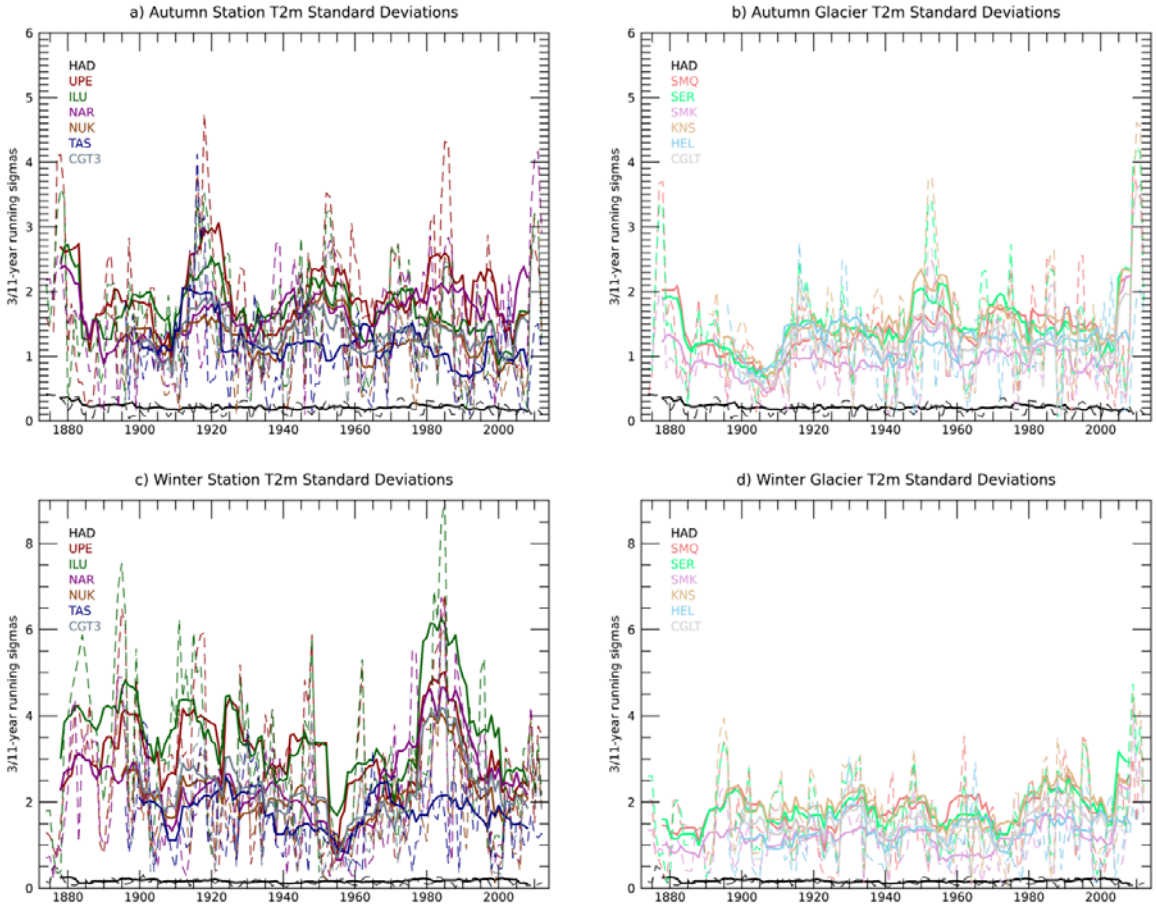

Figure 2 Running 3-year (dashed) and 11-year (solid) standard deviations of autumn Greenland station and glacier time series (a,b) and winter station and glacier time series (c,d). The Northern Hemisphere air temperature series from HADCRUT4 (HAD) is overlaid for reference.

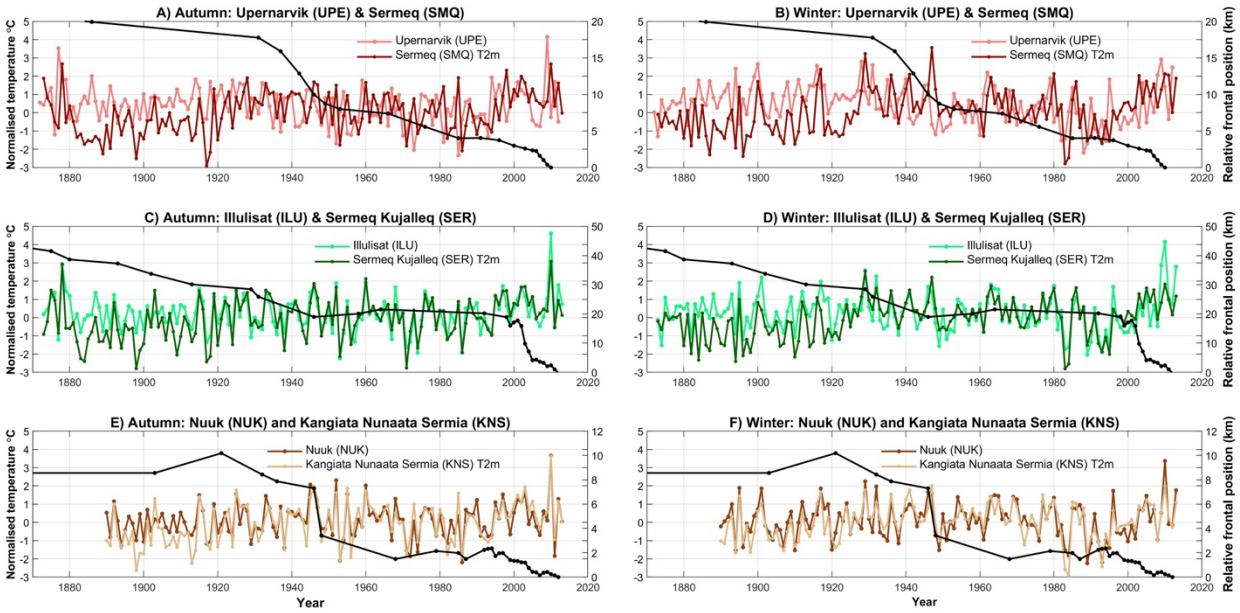

Figure 3 Normalized autumn (OND) and winter (JFM) T2m for Upernavik (UPE) and Sermeq (SMQ) (a,b), Ilulissat (ILU) and Sermeq Kujalleq (SER) (c,d), and Nuuk (NUK) and Kangiaata Nunaata Sermia (KNS) (e,f). Glacier frontal position changes (in km) from multiple observational data sources are also shown (black line) relative to the first available frontal position (e.g., + = advance, - = retreat).

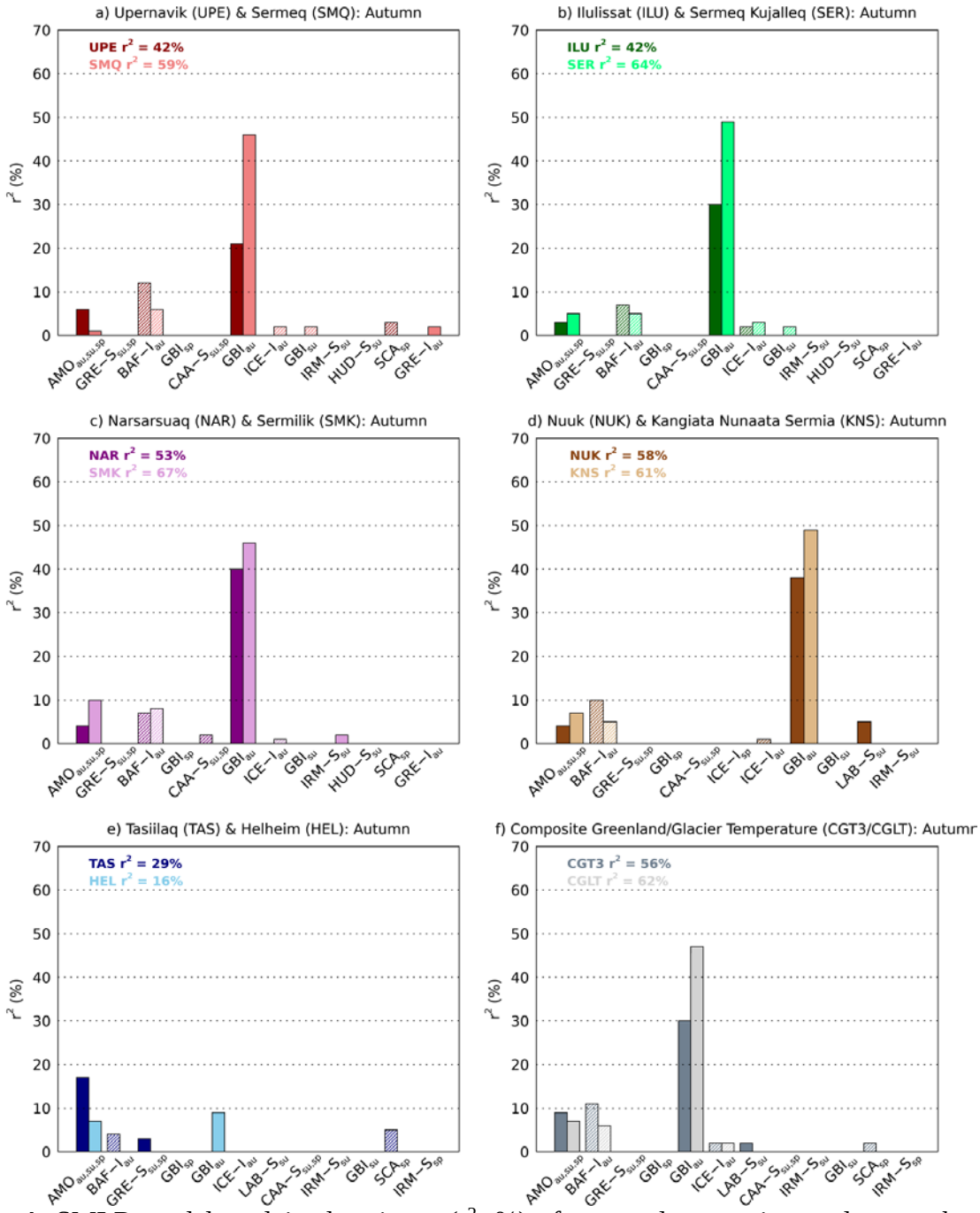

Figure 4 SMLR model-explained variance (r^2; %) of seasonal ocean, ice, and atmosphere PC predictors of autumn (OND) Greenland air temperature variability for nearby coastal and glacier

pairs a) Upernavik (UPE) and Sermeq (SER), b) Ilulissat (ILU) and Sermeq Kujalleq (SER), c) Narsarsuaq (NAR) and Sermilik (SMK), d) Nuuk (NUK) and Kangiata Nunaata Sermia (KNS), e) Tasiilaq (TAS) and Helheim (HEL), and f) Composite Greenland Temperature (CGT3) and Composite Glacier Temperature (CGLT) for full periods of record. Solid (striped) bars represent positive (negative) regression coefficients. Cumulative explained variance is listed in the top left of each plot. Complete descriptions of the x-axis PC predictors are found in **Tables S2–S4**.

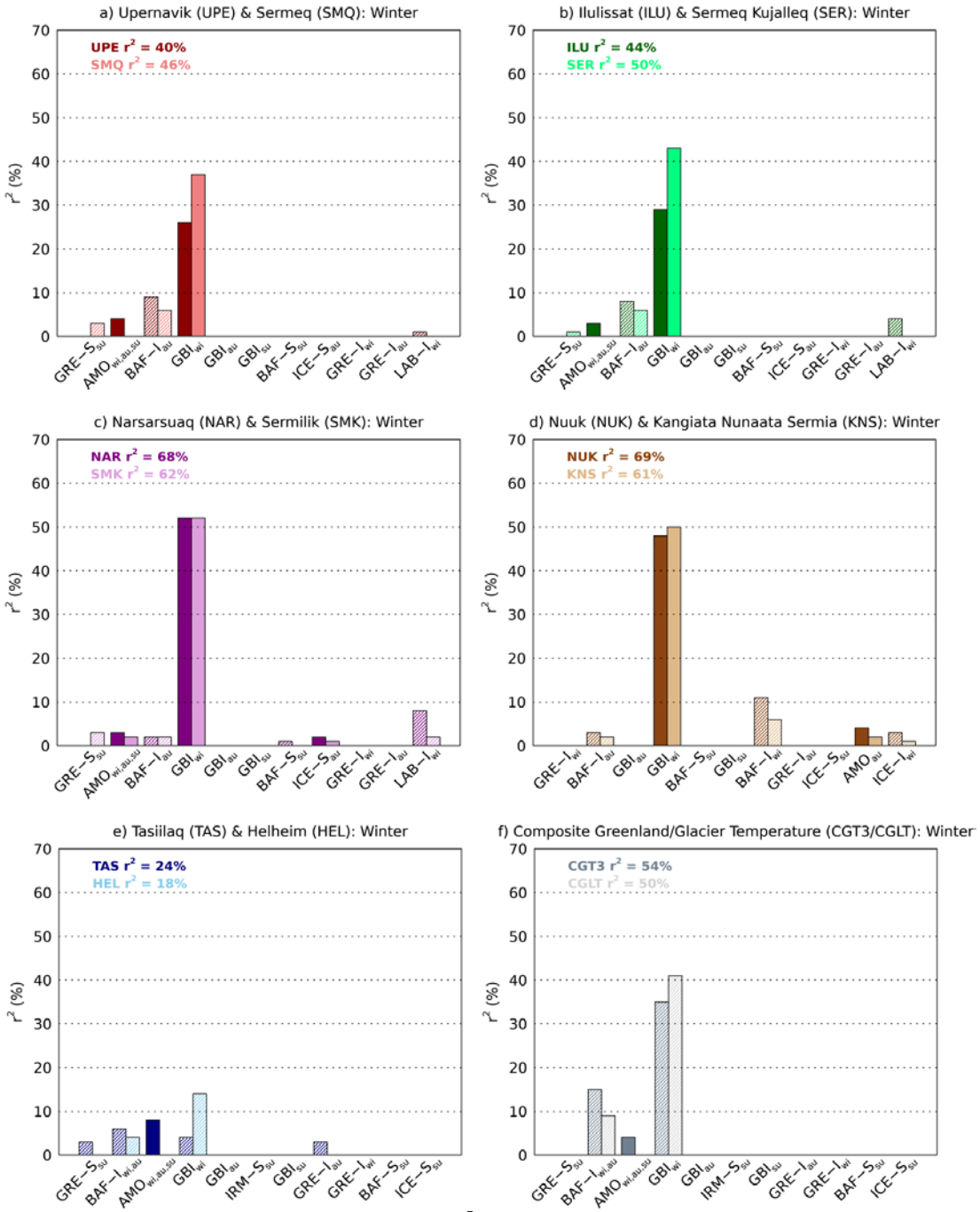

Figure 5 SMLR model-explained variance (r^2; %) of seasonal ocean, ice, and atmosphere PC predictors of winter (OND) Greenland air temperature variability for nearby coastal and glacier

pairs a) Upernavik (UPE) and Sermeq (SER), b) Ilulissat (ILU) and Sermeq Kujalleq (SER), c) Narsarsuaq (NAR) and Sermilik (SMK), d) Nuuk (NUK) and Kangiata Nunaata Sermia (KNS), e) Tasiilaq (TAS) and Helheim (HEL), and f) Composite Greenland Temperature (CGT3) and Composite Glacier Temperature (CGLT) for full periods of record. Solid (striped) bars represent positive (negative) regression coefficients. Cumulative explained variance is listed in the top left of each plot. Complete descriptions of the x-axis PC predictors are found in **Tables S5–S7**.

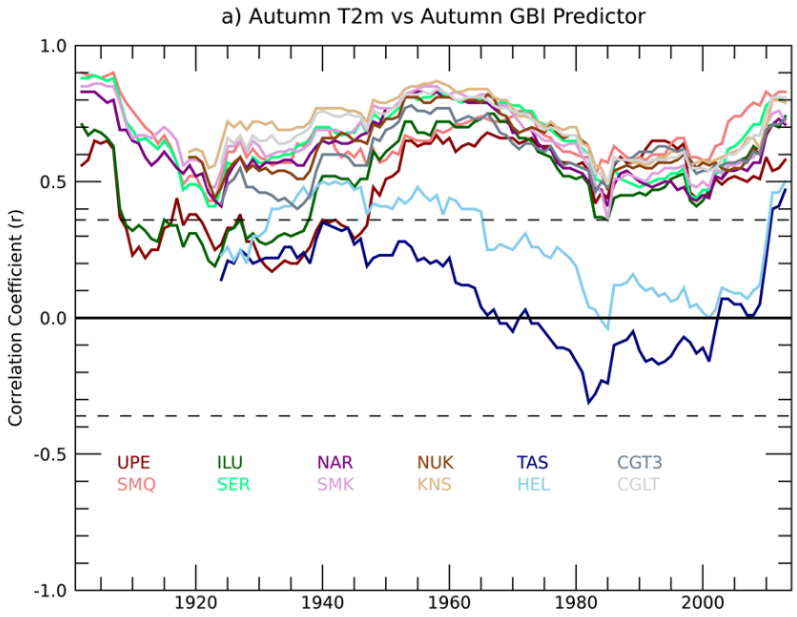

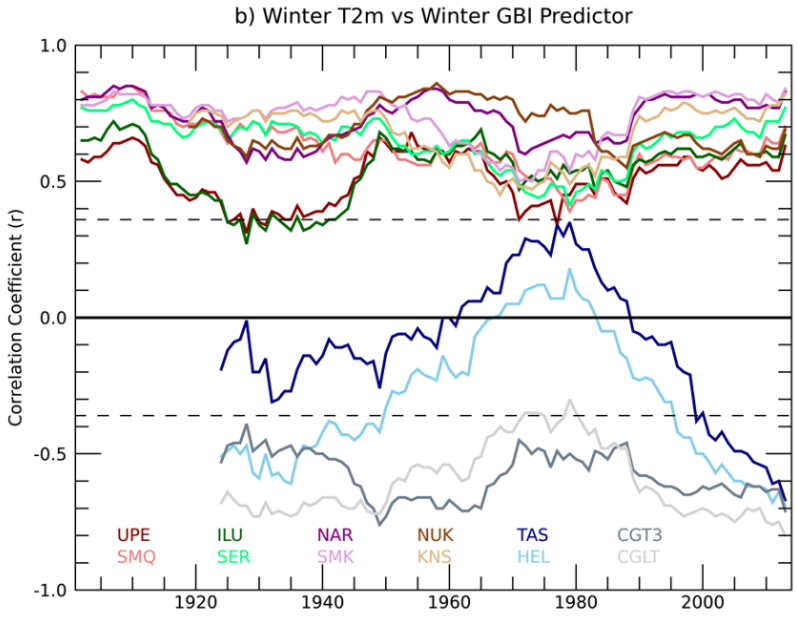

Figure 6 Running 30-year detrended Pearson correlations between the GBI component time series, and the T2m values for a) OND and b) JFM. Except for TAS, parallel season GBI (with NAO) represents the leading PC predictor (see methods for description). Statistically-significant coefficients (for n-2 degrees of freedom; $p \leq 0.05$) measured over discrete 30-year periods are marked by a dashed line where $r > |0.36|$. The initial coefficient for UPE versus GBI JFM in 1902 ($r = +0.56$), for instance, represents a correlation spanning 1873–1902.

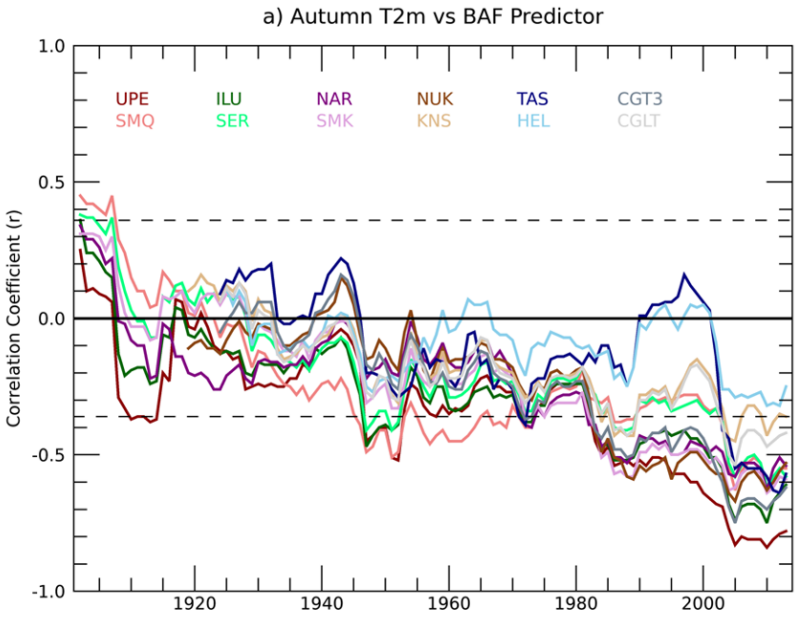

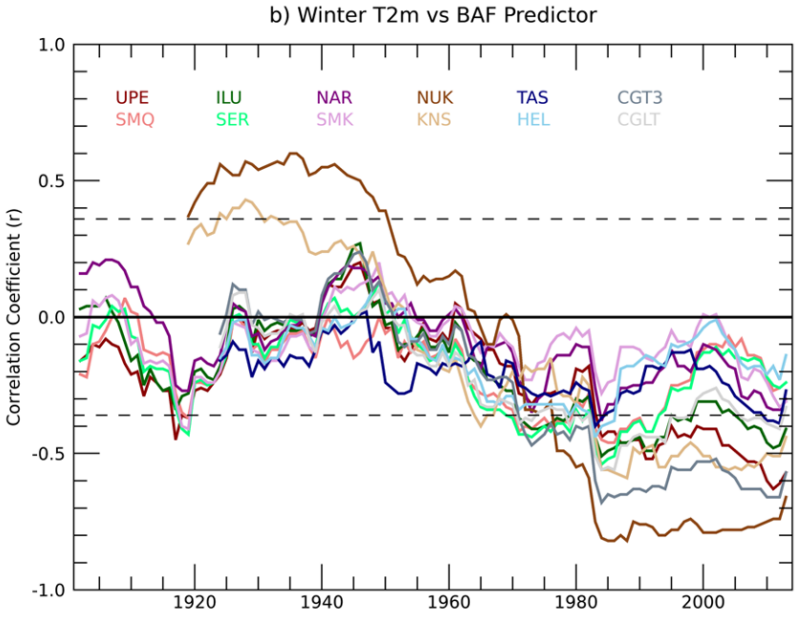

Figure 7 Running 30-year detrended Pearson correlations between the Baffin (BAF) component sea-ice time series, and the T2m values for a) OND and b) JFM. Statistically-significant coefficients (for n-2 degrees of freedom; $p \leq 0.05$) measured over discrete 30-year periods are marked by a dashed line where $r > |0.36|$. The initial coefficient for UPE versus GBI JFM in 1902 ($r=-0.16$), for instance, represents a correlation spanning 1873–1902.

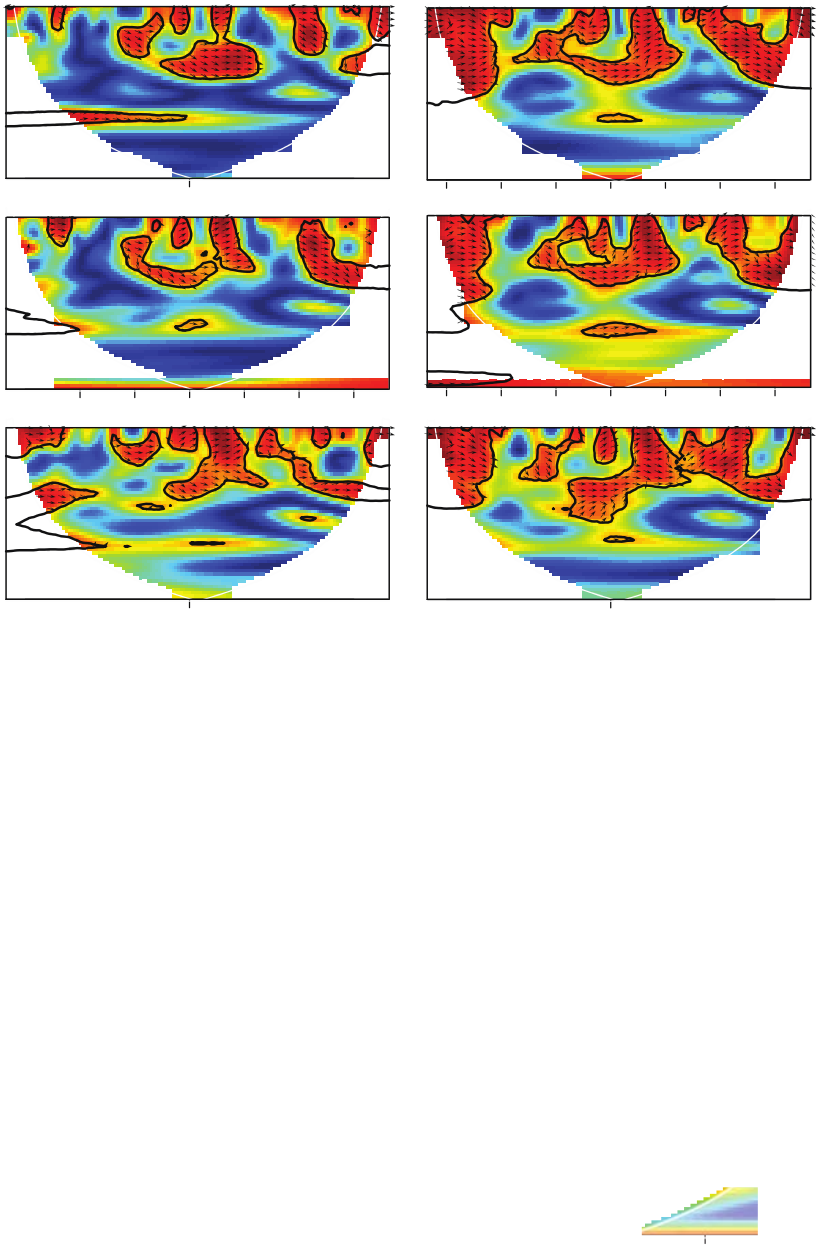

Figure 8 Wavelet coherence between the autumn GBI PC and T2m from a) Upernavik (UPE), b) Sermeq (SMQ), c) Ilulissat (ILU), d) Sermeq Kujalleq (SER), e) Narsarsuaq (NAR), f) Sermilik (SMK), g) Nuuk (NUK), h) Kangiata Nunaata Sermia (KNS), i) Tasiilaq (TAS), j) Helheim (HEL),

k) Composite Greenland Temperature 3 (CGT3), and l) Composite Glacier Temperature (CGLT). Statistically-significant periodicities ($p \leq 0.05$) are shown by contoured areas. The COI is semi-transparent. Phase relationships are shown by the arrows: right-pointing (in-phase); left-pointing (anti-phase); up (temperature lags circulation by 90°); down (temperature leads circulation by 90°). Up and down arrows can also be interpreted as a lead (lag) of 270°.

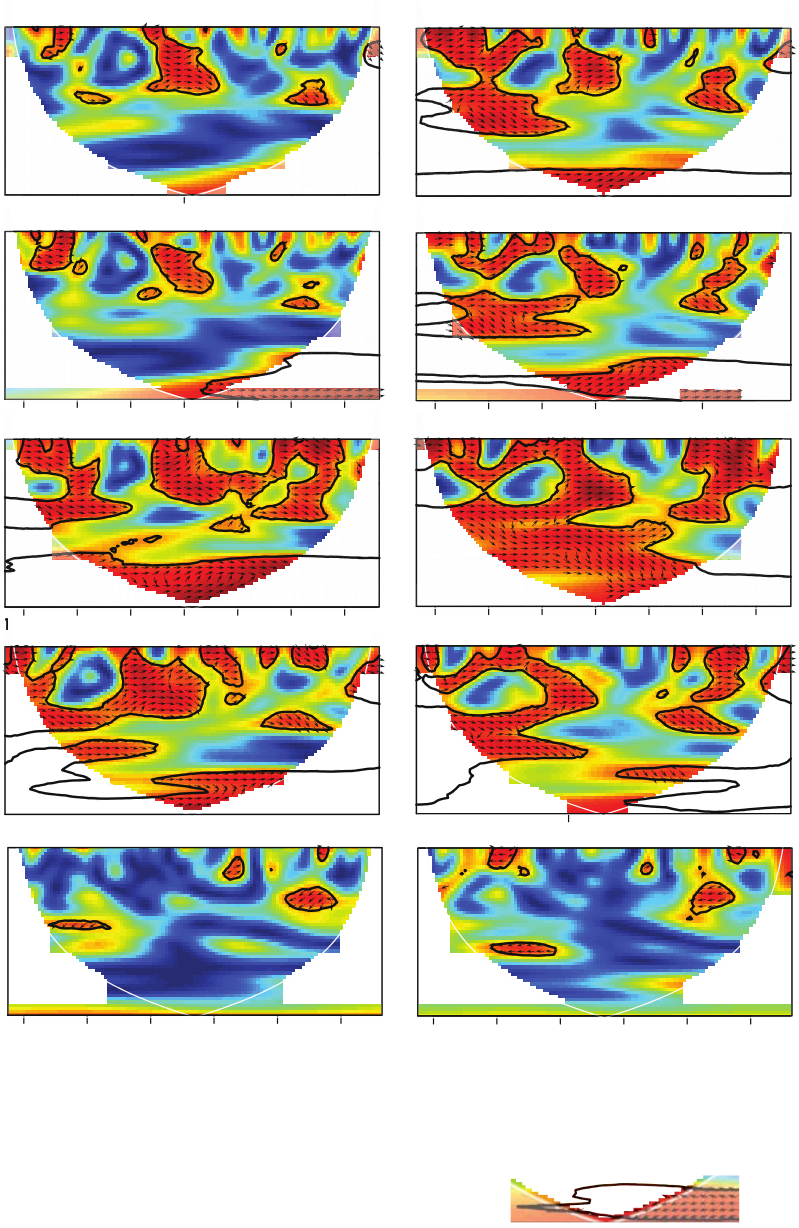

Figure 9 Wavelet coherence between the winter GBI PC and T2m from a) Upernavik (UPE), b) Sermeq (SMQ), c) Ilulissat (ILU), d) Sermeq Kujalleq (SER), e) Narsarsuaq (NAR), f) Sermilik (SMK), g) Nuuk (NUK), h) Kangiata Nunaata Sermia (KNS), i) Tasiilaq (TAS), j) Helheim (HEL),

k) Composite Greenland Temperature 3 (CGT3), and l) Composite Glacier Temperature (CGLT). Statistically-significant periodicities ($p \leq 0.05$) are shown by contoured areas. The COI is semi-transparent. Phase relationships are shown by the arrows: right-pointing (in-phase); left-pointing (anti-phase); up (temperature lags circulation by 90°); down (temperature leads circulation by 90°). Up and down arrows can also be interpreted as a lead (lag) of 270°.